DEEP LEARNING TO ANALYSE 3D TISSUE MORPHOLOGY

ANALYZING THE MORPHOLOGY OF THREE-DIMENSIONAL TISSUE MODELS USING DEEP LEARNING

By: LYAN ABDUL MAJEED ABDUL WADOOD, B.SC

A Thesis Submitted to the School of Graduate Studies in Partial Fulfilment of the Requirements

for the Degree Master of Applied Science

McMaster University MASTER OF APPLIED SCIENCE (2022) Hamilton, Ontario

(Biomedical Engineering)

TITLE: ANALYZING THE MORPHOLOGY OF THREE-DIMENSIONAL TISSUE MODELS USING DEEP LEARNING

AUTHOR: Lyan Abdul Majeed Abdul Wadood, Hons. B.Sc. (McMaster University)
SUPERVISOR: Boyang Zhang, Ph.D.
NUMBER OF PAGES: ix, 58

Lay Abstract

Three-dimensional (3D) tissue models refer to mini-organs grown in labs that exhibit many features of human tissues. Specifically, 3D models can replicate organ structures, which is essential to their function. However, analyzing these structures can be challenging due to limitations with current image analysis tools that are not suited for complex morphologies. To address this limitation, this work focuses on the application of deep learning techniques instead. Deep learning models can learn to identify objects within images and can be trained to recognize the complex structures from bright-field images directly. In this work, we apply deep learning to analyze miniature lung and colon tissues. We demonstrate that these analysis tools can successfully capture changes in the structure of these organ models and apply them for use in several biological studies.

Abstract

Three-dimensional (3D) tissue models, like organoids and spheroids, have been used to recapitulate many characteristics of human tissues. In particular, 3D tissue models can mimic key structural features of the native tissue. However, analyzing the morphology of 3D tissue models is limited by current image analysis tools that extract features like size, contours and texture which cannot fully describe the exhibited morphologies. Instead, deep learning techniques, which can identify objects from images directly can be used to make this type of analysis possible. In this work, we focus on applying deep learning to analyze the 3D tissue morphologies in brightfield images for the first time. Specifically, we developed and validated deep learning models to analyze important structures exhibited by lung spheroids or colon organoids. Deep-LUMEN is a custom deep learning model that can analyze the polarization of lung spheroids. We validated Deep-LUMEN by assessing how the extracellular matrix affects spheroid polarization and how the drug cyclosporin disrupts spheroid assembly. By analyzing the morphological features of lung spheroids, we found that cyclosporin can induce toxic effects at much lower concentrations than expected. This work also presents D-CryptO, a deep learning-based tool that can be used to analyze the structural maturity of colon organoids. D-CryptO analyzes the opacity and the presence of budding structures to assess tissue maturation. We validated D-CryptO by analyzing colon organoid morphology during prolonged culture and short-term perturbation with external stimuli. Additionally, we further applied it to assess organoid morphology following treatment with several chemotherapeutic drugs. Using D-CryptO, we gained insights into potential mechanisms of drug-induced toxicity. Together, these models demonstrate that deep learning is a viable technique to analyze 3D tissue morphology and it can be applied in a broad range of biological studies to gain useful insights into tissue physiology.

Acknowledgements

I would like to thank my supervisor, Dr. Boyang Zhang, for giving me the opportunity to join the lab as an undergraduate student and learn about organ-on-a-chip technology. I sincerely appreciate all the time you dedicated to assisting me with my projects. This work would have not been possible without your continuous guidance and feedback. I would also like to thank my committee members, Dr. Fei Geng and Dr. Hamidreza Mahyar for the valuable inputs that they provided.

I would like to thank all the members of the BZhang Lab. To all the members that contributed to this work, I appreciate all the time and effort that you devoted to these projects. Additionally, I am extremely grateful to all my lab members for the training, support, and encouragement that they provided me with.

I would like to thank the National Sciences and Engineering Research Council of Canada for the funding support. Finally, I am very grateful to my family and friends for their endless support.

Table of Contents

List of Figures

List of Abbreviations

3D	Three-dimensional
Deep-LUMEN	Deep-Learning Uncovered Measurement of Epithelial Networks
CNNs	Convolutional Neural Networks
ECM	Extracellular Matrix
CsA	Cyclosporin A
DMSO	Dimethyl sulfoxide
mAP	mean Average Precision
CFTR	Cystic fibrosis transmembrane conductance regulator

Declaration of Academic Achievement

I declare that the work presented is my own.

Many authors contributed to the work presented in the following chapters and their contributions are detailed within the papers.

Chapter 1: Introduction

The use of cellular models has been instrumental to understand cell physiology *in vivo*. Specifically, 2D cell culture has been extensively used to understand cell biology. These models consist of cells grown on a flat, adherent substrate. While convenient to use and more robust, drug responses, gene expression, and cell shape are inconsistent with *in vivo* tissues, which limits the number of insights that can be gained from these experiments. [1] This also affects the development of new drugs and therapies. For example, many new drugs are recalled in the later stage of clinical trials due to unanticipated toxicity effects.[2] As a result, focus has shifted to creating three-dimensional (3D) tissue models that can better mimic tissue responses *in vivo*. These studies have shown that characteristics like cell proliferation, gene and protein expression levels, and drug effects more closely match human tissues.

A key aspect that 3D models recapitulate is the structure of tissues *in vivo*, which cannot be modelled using 2D culture. For example, epithelial tissues are essential components of organs that provide a barrier to the environment and have specific structures suited for their function.[3] Spheroids are 3D models that can be derived from a broad range of cell types and can self-assemble into polarized structures, which are a common feature of many epithelial tissues, and have been used to study tissue polarization. Previously, spheroids have been used to model the kidney, the liver, and the intestinal epithelium.[4–6] Spheroids can also form disorganized structures with disrupted cell polarity, making them suitable models to study cancers or other disorders affecting cell polarity like ciliopathies.[7] Organoids are alternative tissue mimics, which are derived from stem cells or progenitor tissue, and exhibit organ-specific morphologies.[8] For example, organoids have modelled the regions of the brain, the crypt-villus axis in the small intestine, the crypts in the colon, and the nephron of the kidney.[9–12]

While these morphologies are observable in bright-field images, techniques to analyze and distinguish between them are limited. Analysis can be done manually or through software tools that can extract image features like texture and contours.[13,14] However, these features do not accurately describe the morphologies of the 3D models. Additionally, the differences between the morphologies may not be discernible with these parameters. To address these constraints, deep learning, which is a computer vision technique, could be used. Deep learning models can identify objects within images directly from raw images by learning from a set of training examples.[14] These models are composed of convolutional neural networks which can learn complex, abstract, and biologically relevant features within images. They can also learn the important features that distinguish one morphology from another. Despite these capabilities, deep learning has been previously applied to 3D tissue models for segmentation, detection, and for the replacement of immunofluorescent stains.[15–17] However, deep learning hasn't been applied for the analysis of 3D tissue morphology.

In this work, the objective is to use deep learning to analyze tissue morphologies directly from brightfield images. Specifically, the aims of this project are to (1) identify the unique morphologies present in 3D models (2) develop custom deep learning networks to analyze these morphologies and (3) validate the custom models. The following chapters present the analysis of the morphology in lung spheroids and colon organoids with custom deep learning models. Furthermore, the deep learning models are validated by assessing how perturbations to the cell culture environment influence 3D tissue morphology. Overall, the papers presented follow the same framework but have different literature reviews and methods since different 3D tissue models were used. In both papers, the same instrument was used to acquire images and compile the dataset.

Chapter 2: Application of deep learning to lung spheroids

Spheroids refer to an assembly of cells that have cell-cell and cell-matrix interactions. As a result, spheroids can exhibit cell polarization, and have been used to model the liver, intestine, kidney and have also been used to study tumour biology.[4–6,18] Spheroids have served as useful models to understand polarity, lumen development, and tissue structural disruptions.[7,19] Deep learning analysis of spheroids has been previously applied to analyze polarity in fluorescent images, to analyze spheroid viability following drug treatment, and for spheroid segmentation.[17,20,21] However, deep learning hasn't been used to analyze spheroid structure from brightfield images.

In the following paper, we describe the application of deep learning to analyze the morphology and specifically, the polarization of lung spheroids.[22] To do this, we cultured lung spheroids and acquired images to create a dataset with examples of the morphologies of interest. Next, we developed Deep-LUMEN, an object detection model, by training models with our custom dataset. Finally, we validated Deep-LUMEN by assessing how (1) the extracellular matrix impacts spheroid polarization and (2) the drug, cyclosporin disrupts cell polarization. In this work, we first demonstrated that deep learning could be applied for tissue morphological analysis. We showed that we can train an accurate deep learning model by creating a custom dataset and using transfer learning approaches. Additionally, we demonstrated that Deep-LUMEN could successfully detect changes in morphology. Furthermore, we showed the importance of analyzing morphology as we can gain insights into factors, such as toxic drug effects, that affect spheroid assembly. Several authors contributed to this work and their contributions are outlined on page 17. The work from reference 22 was reproduced with permission from the Royal Society of Chemistry.

Deep-LUMEN Assay – Human lung epithelial spheroid classification from brightfield images using deep learning

Lyan Abdul[1], Shravanthi Rajasekar[2], Dawn S.Y. Lin[2], Sibi Venkatasubramania Raja[3], Alexander Sotra[2], Yuhang Feng[3], Amy Liu[3], and Boyang Zhang[2,4]*

[1]School of Interdisciplinary Science, McMaster University 1280 Main Street West, Hamilton, ON, L8S 4K1, Canada
[2]Department of Chemical Engineering, McMaster University, 1280 Main Street West, Hamilton, ON, L8S 4L8, Canada
[3]Faculty of Health Sciences, McMaster University 1280 Main Street West, Hamilton, ON, L8S 4L8, Canada
[4]School of Biomedical Engineering, McMaster University, 1280 Main Street West, Hamilton, ON, L8S 4L8, Canada

*Correspondence to zhangb97@mcmaster.ca

Keywords: Deep learning; Spheroids; Organoids; Organ-on-a-Chip; Drug testing

Significance of the work:

Deep learning has been applied for the first time to autonomously detect subtle morphological changes in 3D multi-cellular spheroids, such as spheroid polarity, from brightfield images in a label-free manner. The technique has been validated by detecting changes in spheroid morphology in response to changes in extracellular matrices and drug treatments.

Abstract

Three-dimensional (3D) tissue models such as epithelial spheroids or organoids have become popular for pre-clinical drug studies. However, different from 2D monolayer culture, the characterization of 3D tissue models from non-invasive brightfield images is a significant challenge. To address this issue, here we report a Deep-Learning Uncovered Measurement of Epithelial Networks (Deep-LUMEN) assay. Deep-LUMEN is an object detection algorithm that has been fine-tuned to automatically uncover subtle differences in epithelial spheroid

morphology from brightfield images. This algorithm can track changes in the luminal structure of tissue spheroids and distinguish between polarized and non-polarized lung epithelial spheroids. The Deep-LUMEN assay was validated by screening for changes in spheroid epithelial architecture in response to different extracellular matrices and drug treatments. Specifically, we found the dose-dependent toxicity of Cyclosporin can be underestimated if the effect of the drug on tissue morphology is not considered. Hence, Deep-LUMEN could be used to assess drug effects and capture morphological changes in 3D spheroid models in a non-invasive manner.

Introduction

Advances in biological research rely on the use of effective *in vitro* culture systems. By far, the most commonly used approach is to culture primary cells or cell lines on 2D surfaces in a multi-well plate. However, it is generally recognized that the flat and hard plastic substrates commonly used are not representative of the cellular environment found in organisms. For instance, studies have shown that epithelial cells on monolayer culture have compromised integrin function leading to a higher frequency of chromosome mis-segregation during proliferation(1). On the contrary, growing cells within a natural extracellular matrix that permits self-organization in 3D can significantly improve chromosome segregation fidelity(1). Both primary chondrocytes and hepatocytes have also been shown to lose their normal phenotype rapidly once removed from the body and when placed in 2D culture(2, 3). Issues like these significantly limit the potential of 2D culture systems to predict the cellular responses of real organisms.

Recognizing these challenges, 3D tissue culture with tissue-specific architecture, mechanical and biochemical cues, and cell-cell communication could help reduce the gap between cell-based assays and physiological tissues(4). Stem-derived organoids or 3D spheroids are self-

organized multi-cellular tissue grown in 3D hydrogel matrices. Within this 3D environment, cells can sense a substrate that more closely resembles native extracellular matrices and have the freedom to remodel and form 3D organ-specific structures. 3D cancer spheroids have been shown to outperform 2D cell monolayers in drug screening(5). Various organ-specific organoids from the kidney(6), colon(7), brain(8), and liver(9) have shown sophisticated tissue functions that would be impossible to replicate in 2D. For these reasons, 3D spheroid and organoid cultures are fast becoming the ideal model systems for *in vitro* drug testing and biological research.

Despite these advantages, there are barriers to using 3D models for pre-clinical drug testing. High-throughput screening has been optimized for monolayer culture for decades. 3D tissue models often lack automated workflows for analysis with fast processing times[9]. More importantly, characterizing 3D tissue morphological changes in response to drug treatments, even though it can provide highly relevant physiological information that cannot be easily derived from 2D culture, is challenging. Conventional imaging processing techniques, mostly suitable for 2D cultures, fall short in accurately characterizing complex 3D features that are not a simple description of the area, size, or shape, which can be more easily defined. In addition, the 3D environment presents artifacts like overlapping tissues, out of focus tissues, varying light conditions, tissue heterogeneity, or even supporting tissues like vasculatures, which all present significant challenges to conventional imaging processing techniques.

Deep learning could overcome these challenges by circumventing the need to arbitrarily define multiple parameters for any given set of images as in the conventional imaging processing technique. Specifically, convolutional neural networks (CNNs) are a class of deep learning and are mainly used for image analysis. CNNs recognize patterns from large training datasets, emulating the learning process inherent to our brain; hence it does not require any parameter tuning and runs autonomously. A truly myriad of applications has been explored using this

technology. For spheroid and organoid analysis, machine and deep learning have been previously used to (1) localize spheroids and organoids in 3D cultures and determine their diameter(10-12) and (2) to segment spheroids(11). Although epithelial spheroid polarity has been classified by deep learning, this analysis was done on fluorescent images(13). Deep learning has yet to be applied to detect subtle changes in 3D multi-cellular tissue morphology, such as spheroid polarity, from brightfield images in a label-free manner.

Utilizing Tensorflow Object Detection API(14), here we present an open-source algorithm, Deep-Learning Uncovered Measurement of Epithelial Networks (**Deep-LUMEN**), which has been trained by a large dataset to enable users to detect changes in the luminal structure of 3D spheroids automatically. The formation of the lumen is an indication of proper cell polarization, and its disruption is a significant phenotypic change in many tissues. In this validation study, we first trained Deep-LUMEN to classify the polarity of spheroids directly from brightfield images. Then, we validated this algorithm by tracking how spheroid morphology changes in response to different types of extracellular matrices and drug treatment.

Results

Lung alveolar spheroid generation

Lung alveolar epithelial cells (A549), when embedded in a 3D hydrogel matrix (such as Matrigel® or Fibrin gel), can proliferate and self-organize into a 3D spheroid over time. However, influenced by the culture environment, only a fraction of the population will self-organize into spheroids with a hollow lumen, which is the correct morphology of lung alveoli. Therefore, tracking this morphological feature could allow us to predict the changes in the health and function of the lung alveolar epithelium in response to environmental cues and drug treatment (**Figure 1a**). Utilizing this self-assembly process, we developed the lung spheroid models by casting single-cell suspension in Matrigel® in standard 384-well plates (**Figure 1b**).

The high-throughput 384-well plate, coupled with a high-content image cytometer, allowed us to automate the image acquisition process and collect thousands of brightfield images. Images were taken at different planes (spaced 50 μm apart) through the z-axis to capture all the spheroids in the scanned volumetric space (**Figure 1c**).

Training dataset generation

We created a custom training dataset containing 4000 images (14,993 examples of no lumen and 2,351 examples of lumen spheroids). Out of focus spheroids were omitted from each image to avoid double-counting. Any abnormal morphologies or monolayer formations were also omitted (**Figure 1d**). Bounding boxes were drawn around the in-focused spheroids and categorized accordingly. A spheroid was categorized as "lumen" if there was a prominent indent in the center of the spheroid. Otherwise, the spheroid was given a "no lumen" classification. Immunofluorescent staining confirms that lumen formation is directly correlated to this indent feature from brightfield images and also correlates to cell polarization and the proper organization of the lung alveolar cells. Stronger F-actin staining was seen on the apical side of the luminal spheroid, while disorganized spheroids showed intense F-actin staining on both basal and apical sides (**Figure 1d**, **Supplementary Figure 1**). It's important to note that even though the immunofluorescent staining validated our assumption, the immunofluorescent assay is terminal. On the contrary, Deep-LUMEN classification from brightfield images is non-invasive and continuous. In addition, changes in spheroid morphology can be automatically assessed for each image present in the z-stack, providing a characterization of spheroid morphology through the entire hydrogel (**Figure 1e**). The full training dataset, including the images and annotations, are publicly available at https://osf.io/g2a7r/

Model optimization

After training, the performance of the algorithms were then tested on a set of one-hundred and ninety-seven new images. The models outputted bounding boxes around spheroids along with the classification and the confidence probability. Furthermore, the algorithms learned to omit out-of-focus spheroids and spheroids of abnormal shape (**Figure 2a**). To get the best results, we tested five different pre-trained models and fine-tuned them on our lung spheroid dataset(15-18). Out of the five models (Model 1-5, **Figure 2b**), Faster R-CNN with ResNet101 (Model 5) performed the best. When tested with a new test-set (197 new images) it had a 73% mean average precision (**Figure 2d**) along with the fewest false positives and false negatives (**Figure 2c**). To further improve this model's performance, we then added additional data augmentation options to generate Model 6. When tested with the test-set images, Model 6 (Faster R-CNN ResNet101 with data augmentation) had a 83% mean average precision (**Figure 2e**), detected the highest number of "lumen" and "no lumen" spheroids, and had a lower rate of false positives and false negatives (**Figure 2c**). Therefore, this Model 6 was used at the end and is referred to as Deep-LUMEN. Overall, the analysis and classification of spheroids using Deep-LUMEN were more than 20 times faster than manual labeling (**Figure 2f**). Additionally, Deep-LUMEN outputs confidence scores for each of its predictions. We observed that the score corresponded with the extent of lumen development. For the non-polarized spheroids, the confidence decreases when an indentation is present. For the polarized spheroids, the confidence increases as the indentation becomes larger and the lumen is more well-defined (**Figure 2g**). This observation indicates that it could be possible to further stratify the stages of spheroid lumen development based on the confidence score.

Spheroid morphological changes in response to extracellular matrices

We then used Deep-LUMEN to assess the morphological changes of lung spheroids in response to different extracellular matrices (ECM). Lung alveolar epithelial spheroids were embedded in four different hydrogel conditions and cultured for 12 days in a standard 384-well plate (**Figure**

3a). In all conditions, the alveolar epithelial cells started to proliferate, and the diameter of the spheroids increased over time (**Figure 3b).** There were no significant differences between the different groups. However, the percentage of polarized spheroids (spheroids containing a lumen) in 10 mg/mL fibrin on Day 8 was significantly lower than in the Matrigel® condition (**Figure 3c**). This suggests an interplay of signals between the Matrigel® and the epithelial cells allowing for the formation of the lumen by guiding epithelial polarization. It is well known that laminin, a major component of the basement membrane and also abundant in Matrigel® are integral for guiding cells to develop the polarity required for lumen formation(19). Therefore, we found Matrigel® to be optimal for lung spheroid culture. The unique aspect of this study is that we were able to make this conclusion by analyzing just the brightfield images with Deep-LUMEN in a completely non-invasive manner. It is also clear that we would not be able to capture this effect should we have solely focused on quantifying spheroid diameters using conventional image analysis methods.

Spheroid morphological changes in response to drug treatment

Lastly, we examined how drug treatment could affect lumen formation in the lung alveolar spheroids. Cyclosporin A (CsA) is an immunosuppressant medication used after organ transplantation(20) and for other autoimmune conditions such as rheumatoid arthritis(21), psoriasis(22), etc. However, at higher dosages, it is known to be toxic to kidney or liver cells. Many studies have shown that a dosage above 10 μM (around 100 μM) is required to observe a significant toxic effect from CsA on liver or kidney epithelial cells in vitro(23, 24). Here we tested CsA over a wide concentration range from 0.01 to 10 μM (**Figure 4a**). We found that at 10μM the ability of the cells to self-organize into a hollow alveolar spheroid is already compromised, even though there is no significant effect on the size and number of lung spheroids due to CsA which indicates the drug is yet to compromise cell viability (**Figure 4 b-**

d). While spheroids will, by default, develop more lumens over time, the group treated with 10μM CsA failed to form more luminal spheroids and resulted in a drastic decrease in luminal spheroid count compared to the control three days after drug administration (**Figure 4e**). This suggests that the effective toxicity of CsA could be much lower than initially expected. This further highlights the need to examine higher-level tissue morphological changes in addition to the more obvious toxicity effect on cell viability and growth in drug testing.

Discussions

Object detection and classification, primarily based on subtle changes in morphological features, is a challenging task but needed if we want to fully explore the benefits of 3D models in biological research. In this study, we hope to lay the groundwork to help further apply machine learning to analyze more complex tissue models. Specifically, we showed that by offering a closer look at the changes in tissue morphology, deep learning could help improve the sensitivity of tissue models to drug treatments.

Because the Deep-LUMEN algorithm was not just localizing the spheroids, it's important to note that the collection of z-stacked brightfield images and the ability to eliminate out-of-focus spheroids is critical for avoiding double counting and for accurately classifying the spheroids, as out-of-focus spheroids will not contain sufficient morphological details to allow accurate characterization. The z-stack scanning capability is a common feature in most high-content cytometers used for high-throughput screening. Also, the Deep-LUMEN program does not require any preprocessing on the images, and both spheroid detection and classification occur in a single step to streamline the analysis process. Given the fast analysis speed, it's possible to integrate the Deep-LUMEN analysis in real-time during image acquisition and under live view to guide image selection.

Lumen formation is a gradual process in which a smaller lumen appears first and then gradually enlarges. Although we didn't quantify the size of the inner lumens of our spheroids over time, we did notice that the degree of confidence automatically provided by the Deep-LUMEN algorithm seems to correlate with the extent of lumen development. Freshly formed lumens with small luminal diameters are often given a confidence of around 85%, while well-developed lumens are assigned a confidence of about 99%. This indicates that even more minute differences in tissue morphology could be discernable. In future studies, rather than limiting 3D model characterization to a two-category classification, additional characteristic parameters, where the gradual change in tissue morphology is transformed into a range of quantifiable values, could be further explored.

Limitations

The accuracy of our trained model could be further improved with additional training images. However, because much more images can be analyzed with Deep-LUMEN compared to manual analysis, our current level of accuracy didn't impact the outcome of our experimental analysis, where we can successfully capture the effect of drugs and matrix. Finally, in this study we have only used one type of image cytometer for image acquisition. Image contrast and the filter used could vary between different image cytometers. In future studies, it would be interesting to see if models trained using training images collected from one cytometer can be used for images collected from a different cytometer even when the tissue culture platform is the same. This feature will impact the feasibility of distributing a trained model to different labs with very different imaging infrastructures.

Conclusions

We have developed a deep learning model, called Deep-LUMEN, that can be used to detect morphological changes in lung epithelial spheroids. We demonstrated that it is possible to

develop object detection programs to recognize subtle changes in 3D tissue morphology in response to ECMs and drug treatment. We envision this approach could help accelerate the transition to 3D tissue models for high-throughput drug screening by making the image analysis process less invasive and more informative.

Materials and Methods

Cell Culture

A549 cells purchased from Cedarlane labs (Cat# PTA-6231) were cultured in Hams F12K media (Cedarlane labs, Cat# 302004), supplemented with 10% of Fetal Bovine Serum (Wisent Bioproducts, Cat# 098-150), 1% of Penicillin-Streptomycin solution (100X) (Wisent Bioproducts, Cat# 450-201-EL) and 1% of HEPES solution (1M) (Wisent Bioproducts, 330-050-EL). Cells were cultured until 90% confluence in T75 flasks (5% CO_2, 37 °C). The A549 cells used for all the experiments were between passage 2-5. Before cell seeding, all cells were strained using 40μm cell strainers to remove any cell clumps and get a uniform single-cell suspension.

Lung spheroid culture

To generate lung spheroids, A549 cells were mixed with growth-factor reduced Matrigel® (Corning, Cat# CACB356231) at a seeding density of 0.1 million cells/ml. 25 μL of this mixture was cast onto one well of a standard 384-well plate (VWR, Cat# 10814-226). For ECM optimization experiments, the cells were also suspended in Fibrin gel. To prepare the fibrin gel, 125 μl of fibrinogen gel aliquot was mixed with 25 μL of thrombin (1.5 U/ml) before gel casting. Both fibrinogen and thrombin stock solutions were prepared as per the supplier's guidelines (Sigma Aldrich, Cat# F3879-1G, T6884-100UN). Similar to Matrigel® condition, 0.1 million cells/ml were suspended in different concentrations of Fibrin gel (2 mg/ml, 5 mg/ml,

and 10 mg/ml), and 25 μL of the final gel mixture was cast into each well. The spheroid culture was maintained for up to 10 days in 5% CO_2 and 37°C. Culture media was changed every two days.

Immunofluorescent staining of lung spheroids

Cultured lung spheroids were first washed with 1X PBS to remove residual culture media. The tissue was then fixed with 10% Formalin solution overnight in 4°C. The fixative was removed, and the tissue was washed three times with 1X PBS and blocked overnight in 4°C with 10% Fetal Bovine Serum. The tissue was then stained with F-actin conjugate antibody (Cedarlane Labs, Cat#20553-300) along with DAPI (Sigma Aldrich, Cat#D9542-5MG) and incubated overnight in 4°C. Both antibodies were diluted at 1:200 ratio in PBS with 2% (v/v) FBS. After antibody incubation, the samples were washed in PBS overnight and imaged using an image cytometer.

TensorFlow Object Detection API Configuration

Image annotations were created using the labeling program. For each image, boxes were drawn around the spheroids and categorized accordingly. The annotations were converted into .xml files containing the bounding box coordinates and the class name for each labeled spheroid. A label map that assigns an integer to each class was also created in a .pbtxt file. Through the use of helper scripts, the annotations were converted into the TFRecord File format. From the TensorFlow detection model zoo, the pre-trained models were downloaded along with their corresponding configuration files. For model 3, 4, and 5: the following changes were made to the configuration file. The number of classes field was set to 2 and the image dimensions field was set to match the images' dimensions (1224 × 904 pixels). For model 1, and 2, the number of classes was set to 2 and the image dimensions were set to 612 x 452 pixels and 640 x 640

pixels respectively. Finally, for all models, training was set to 200,000 steps. The location of the pre-trained model, the datasets, and the label maps were set.

Model training was conducted using Google Colaboratory. The training was executed on either a Nvidia K80, T4, P4, or P100 GPU, which was randomly assigned with each connection to the Google Colaboratory GPU backend. For model 6, the following data augmentation options were added: random_adjust_brightness, random_adjust_contrast, random_adjust_hue, random_distort color, random_vertical_flip, and random_rotation90. The final lung spheroid training dataset consisted of 3617 images, the validation set consisted of 391 images and the test set contained 197 images.

Image Acquisition

Lung spheroids were fixed following eight to ten days of culture. The Cytation 5 Cell Imaging Multi-Mode reader (BioTek® Instruments) was used to take z-stack images of the spheroids with a 50 µm step size. Brightfield images were captured under 4X magnification. To capture spheroids from the entire well, images from four different regions of each well were acquired. One well produced 128 total images in .tiff formats. The .tiff images were renamed and simultaneously converted into RGB and .jpg format using a macro script on ImageJ. For fluorescent images and their corresponding brightfield images, the magnification used was 10X.

Drug administration studies

Cyclosporin A was purchased from Sigma Aldrich (Cat# 30024-25MG). The drug stock solutions were prepared as per the manufacturer's instructions. The drug was dissolved in Dimethyl sulfoxide (DMSO) (Sigma Aldrich, Cat# D2650-5X5ML) to get a concentration of 25 mg/mL and was then sterile-filtered using a syringe with a filter insert (VWR, Cat# CA28145-501). This solution was diluted 1000 times in culture media to achieve a final DMSO

concentration that was lower than 0.1%. Serial dilutions were performed in culture media to get the four concentrations: 10, 1, 0.1, and 0.01 µM. Cyclosporin A was administered for seven days. The drug solutions were refreshed every other day. Z-stack images of 4X magnification were taken every day using Cytation 5 Cell Imaging-multi mode reader.

Quantification analysis

To evaluate the models based on the number of class instances detected, 197 new test images were chosen and annotated. These served as the ground-truth detections. The detections from each trained model were outputted on these new test images. A detection was considered "correct" if the spheroid was labeled in the ground-truth annotation, and the label matched the ground-truth classification. To measure time to output detections, a human annotator and the model were timed labeling 25 images. The mean Average Precision (mAP) at a 50% intersection of union, using the Pascal VOC performance metrics, was used to measure accuracy. To obtain mAP, a test set was created and each model was analyzed with this test set. To measure the effect of extracellular matrices on spheroid diameter, at least six in-focus spheroids from each condition on day 1, 6, and 10 of culture were measured using ImageJ. To determine the effect of CsA on spheroid diameter, the x-axis bounding box coordinates for all detections above a 50% score confidence were outputted and subtracted from each other. This was done for at least three wells. To assess the effect of CsA on the total number of spheroids and the percentage of lumen spheroids, the width of the bounding boxes were filtered by class and extracted for three independent samples.

Statistical Analysis

All data are expressed as mean ± standard deviation. Statistical tests conducted were either one-way ANOVA, two-way ANOVA, or one-way ANOVA on ranks followed by the Holm-Sidak or Dunn's method. For one-way and two-way ANOVA, requirements of normality and equal

variance were met. Results were considered significant when a p-value of less than 0.05 was obtained.

Data Availability

All the trained models and the datasets can be downloaded from https://osf.io/g2a7r/

Acknowledgments

This work was funded by the National Sciences and Engineering Research Council of Canada (NSERC) Undergraduate Research Award to LA, and Canadian Institute of Health Research (CIHR) Project Grant (PJT-166052) to BZ. The authors are grateful to all the contributors to the Tensorflow Object Detection API and the contributors to BioRender.com which we have used to make the illustrations in this work. Lastly, the authors are grateful to all the essential frontline workers fighting COVID-19.

Author contribution

L.A. performed the experiments, deep learning analysis, and prepared the manuscript. S.R. contributed to the experiments and prepared the manuscript. D.S.Y.L. contributed to the fluorescent staining of the spheroids. S.V.R and Y.F. contributed to image annotation and quantitative analyses. A.S. and A.L. contributed to image acquisitions. B.Z. envisioned the concept, supervised the work and prepared the manuscript.

Competing financial interests

None.

References

1. Knouse KA, Lopez KE, Bachofner M, Amon A. Chromosome Segregation Fidelity in Epithelia Requires Tissue Architecture. Cell. 2018;175(1):200-11.e13.

2. Bierwolf J, Lutgehetmann M, Feng K, Erbes J, Deichmann S, Toronyi E, et al. Primary rat hepatocyte culture on 3D nanofibrous polymer scaffolds for toxicology and pharmaceutical research. Biotechnology and bioengineering. 2011;108(1):141-50.
3. Von Der Mark K, Gauss V, Von Der Mark H, Müller P. Relationship between cell shape and type of collagen synthesised as chondrocytes lose their cartilage phenotype in culture. Nature. 1977;267(5611):531-2.
4. Yamada KM, Cukierman E. Modeling tissue morphogenesis and cancer in 3D. Cell. 2007;130(4):601-10.
5. Kota S, Hou S, Guerrant W, Madoux F, Troutman S, Fernandez-Vega V, et al. A novel three-dimensional high-throughput screening approach identifies inducers of a mutant KRAS selective lethal phenotype. Oncogene. 2018:1.
6. Low JH, Li P, Chew EGY, Zhou B, Suzuki K, Zhang T, et al. Generation of Human PSC-Derived Kidney Organoids with Patterned Nephron Segments and a De Novo Vascular Network. Cell Stem Cell. 2019.
7. Matano M, Date S, Shimokawa M, Takano A, Fujii M, Ohta Y, et al. Modeling colorectal cancer using CRISPR-Cas9–mediated engineering of human intestinal organoids. Nature medicine. 2015;21(3):256.
8. Qian X, Nguyen HN, Song MM, Hadiono C, Ogden SC, Hammack C, et al. Brain-region-specific organoids using mini-bioreactors for modeling ZIKV exposure. Cell. 2016;165(5):1238-54.
9. Takebe T, Sekine K, Enomura M, Koike H, Kimura M, Ogaeri T, et al. Vascularized and functional human liver from an iPSC-derived organ bud transplant. Nature. 2013;499(7459):481.
10. Bayramoglu N, Kaakinen M, Eklund L, Åkerfelt M, Nees M, Kannala J, et al., editors. Detection of tumor cell spheroids from co-cultures using phase contrast images and machine learning approach. 2014 22nd International Conference on Pattern Recognition; 2014: IEEE.
11. Kecheril Sadanandan S, Karlsson J, Wahlby C, editors. Spheroid segmentation using multiscale deep adversarial networks. Proceedings of the IEEE International Conference on Computer Vision Workshops; 2017.
12. Kassis T, Hernandez-Gordillo V, Langer R, Griffith LG. orgaQuant: Human intestinal organoid Localization and Quantification Using Deep convolutional neural networks. Scientific reports. 2019;9(1):1-7.
13. Soetje B, Fuellekrug J, Haffner D, Ziegler WH. Application and Comparison of Supervised Learning Strategies to Classify Polarity of Epithelial Cell Spheroids in 3D Culture. Frontiers in Genetics. 2020;11:248.
14. Fathi A, Korattikara A, Sun C, Fischer I, Huang J, Murphy K, et al. Speed and accuracy trade-offs for modern convolutional object detectors. 2017.
15. Dai J, Li Y, He K, Sun J, editors. R-fcn: Object detection via region-based fully convolutional networks. Advances in neural information processing systems; 2016.
16. Ren S, He K, Girshick R, Sun J, editors. Faster r-cnn: Towards real-time object detection with region proposal networks. Advances in neural information processing systems; 2015.
17. Liu W, Anguelov D, Erhan D, Szegedy C, Reed S, Fu C-Y, et al., editors. Ssd: Single shot multibox detector. European conference on computer vision; 2016: Springer.
18. Lin T-Y, Goyal P, Girshick R, He K, Dollár P, editors. Focal loss for dense object detection. Proceedings of the IEEE international conference on computer vision; 2017.

19. O'Brien LE, Jou T-S, Pollack AL, Zhang Q, Hansen SH, Yurchenco P, et al. Rac1 orientates epithelial apical polarity through effects on basolateral laminin assembly. Nature cell biology. 2001;3(9):831-8.
20. Nussenblatt RB, Palestine AG. Cyclosporine: immunology, pharmacology and therapeutic uses. Survey of ophthalmology. 1986;31(3):159-69.
21. Wells GA, Haguenauer D, Shea B, Suarez-Almazor ME, Welch V, Tugwell P, et al. Cyclosporine for treating rheumatoid arthritis. Cochrane Database of Systematic Reviews. 1998(2).
22. Ellis CN, Gorsulowsky DC, Hamilton TA, Billings JK, Brown MD, Headington JT, et al. Cyclosporine improves psoriasis in a double-blind study. Jama. 1986;256(22):3110-6.
23. Gerets H, Tilmant K, Gerin B, Chanteux H, Depelchin B, Dhalluin S, et al. Characterization of primary human hepatocytes, HepG2 cells, and HepaRG cells at the mRNA level and CYP activity in response to inducers and their predictivity for the detection of human hepatotoxins. Cell biology and toxicology. 2012;28(2):69-87.
24. Homan KA, Kolesky DB, Skylar-Scott MA, Herrmann J, Obuobi H, Moisan A, et al. Bioprinting of 3D convoluted renal proximal tubules on perfusable chips. Scientific reports. 2016;6:34845.

Figures

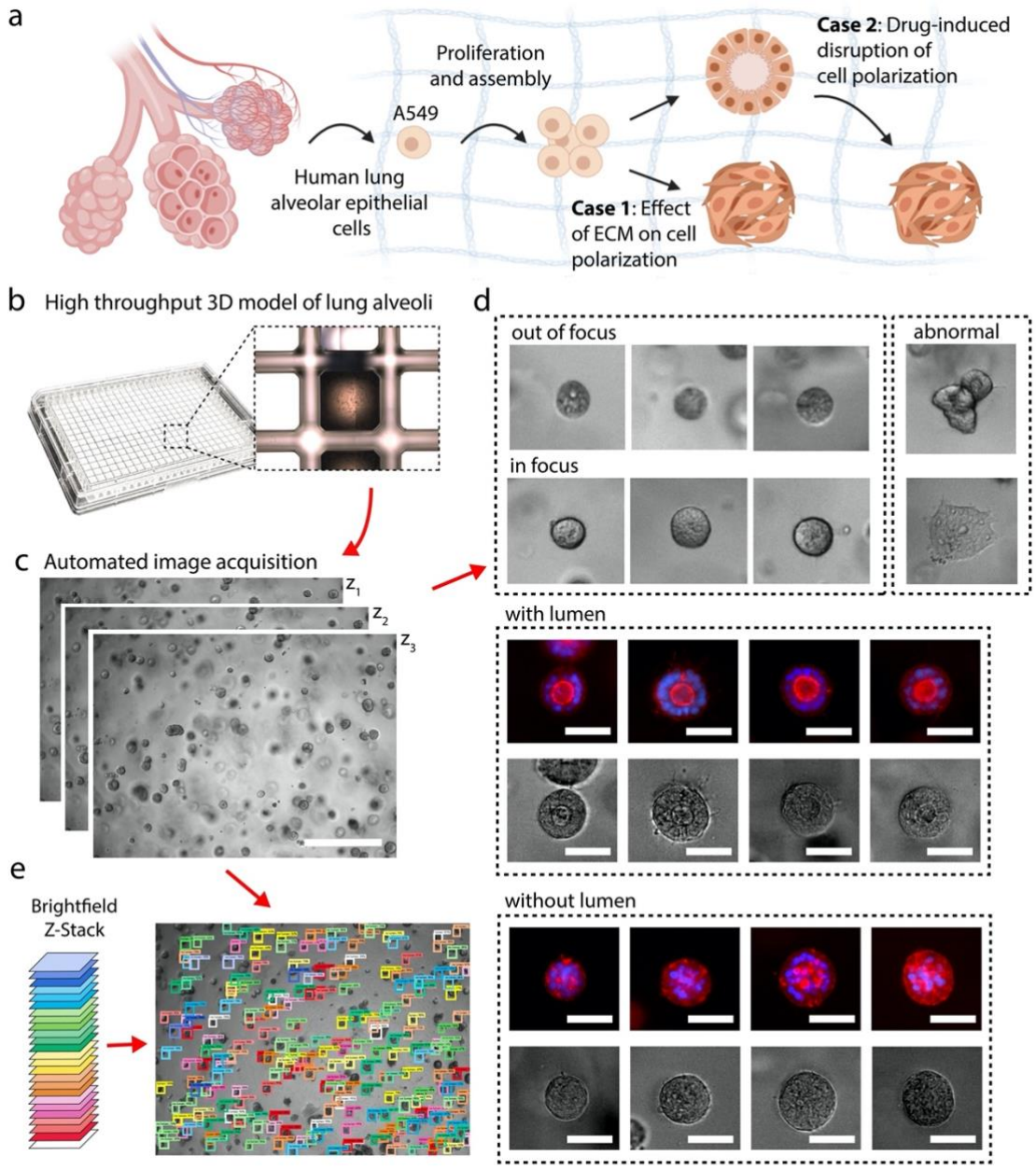

Figure 1. Differential formation of hollow lung alveolar spheroids. a, Illustration of lung epithelial cells proliferating and assembling into either hollow or solid spheroids in a 3D matrix. **b**, Tissue culture setup where 25µL of Matrigel® embedded with cells are cast in standard 384-well plates. **c**, acquired z-stack transmission-light images. **d**, Example scenarios of lung spheroids seen from the collected images. Corresponding fluorescent images stained for F-actin (red) and DAPI (blue) of lung spheroids with or without a lumen (representative images from n=6 samples). Scale bar, 50 µm. **e**, z-stack acquisition allows for spheroid morphology assessment throughout entire hydrogel. Spheroids on different focal planes were detected with developed Deep-LUMEN algorithm from z-stack images and then labeled with different colors for visualization.

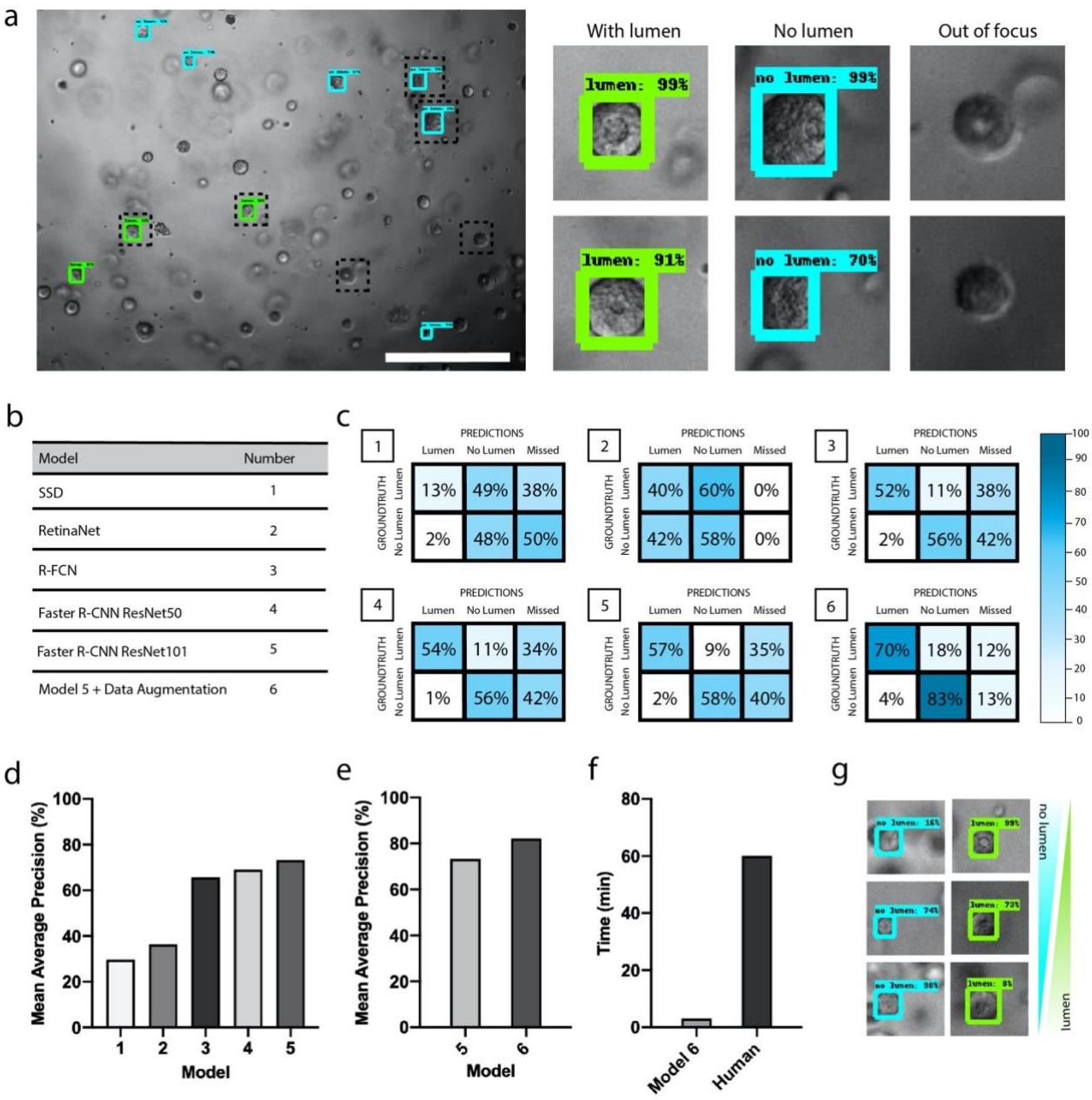

Figure 2. Optimization of model performance. a, Detection output of Deep-LUMEN following fine-tuning with custom dataset. Bright-field images were obtained by taking 4X z-stack images of lung spheroids cultured in Matrigel®. Scale bar, 500 μm. **b,** Models used and their corresponding Model number. **c,** Confusion matrix for each trained model outlining the true positives, the true negatives, the false positives and the false negatives. Assessment of accuracy was performed on 197 new test images. **d,** mAP metric for each fine-tuned model. **e**, Comparison of model 5 performance with and without data augmentation. Model 6 (model 5 with data augmentation) was chosen as the final model and will be referred to as Deep-LUMEN. **e,** Comparison of the time required to localize and classify spheroids in 25 images between Deep-LUMEN (on a GPU) and human annotators. **g,** Deep-LUMEN's confidence scores reflect the extent of lumen formation.

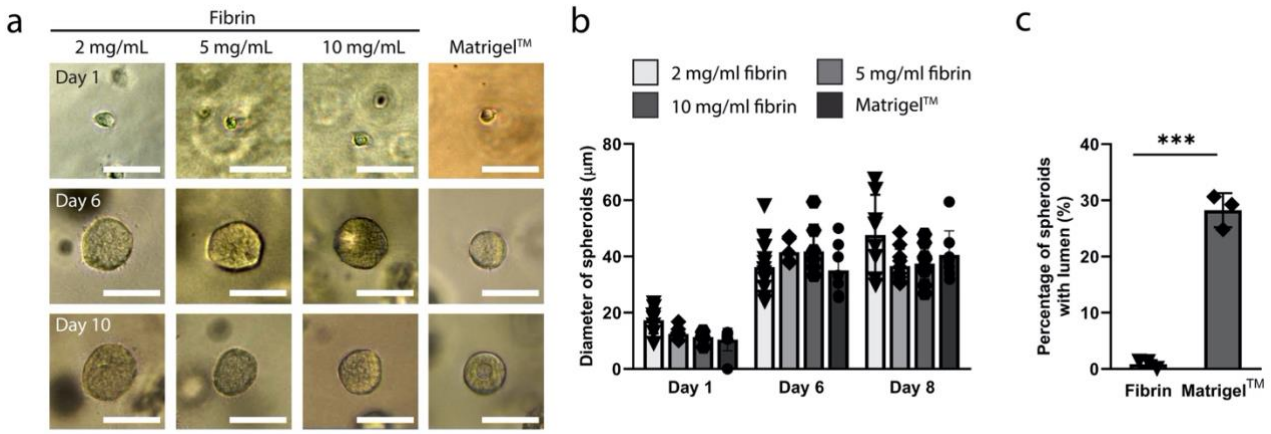

Figure 3. Spheroid morphological changes in response to extracellular matrices a, Assembly of lung alveolar epithelial cells into spheroids in different ECM conditions. **b,** Quantification of the diameter of spheroids in different ECM conditions (n= 6 to 18 spheroids). No significant differences were found. Statistical significance was determined using one-way ANOVA on ranks with Dunn's method. **c,** Quantification of the percentage of spheroids with the presence of lumen using Deep-LUMEN in 10 mg/ml fibrin and Matrigel® (n=3). Statistical significance was determined using one-way ANOVA with the Holm-Sidak method.
*$p < 0.05$, **$p < 0.01$, ***$p < 0.001$.

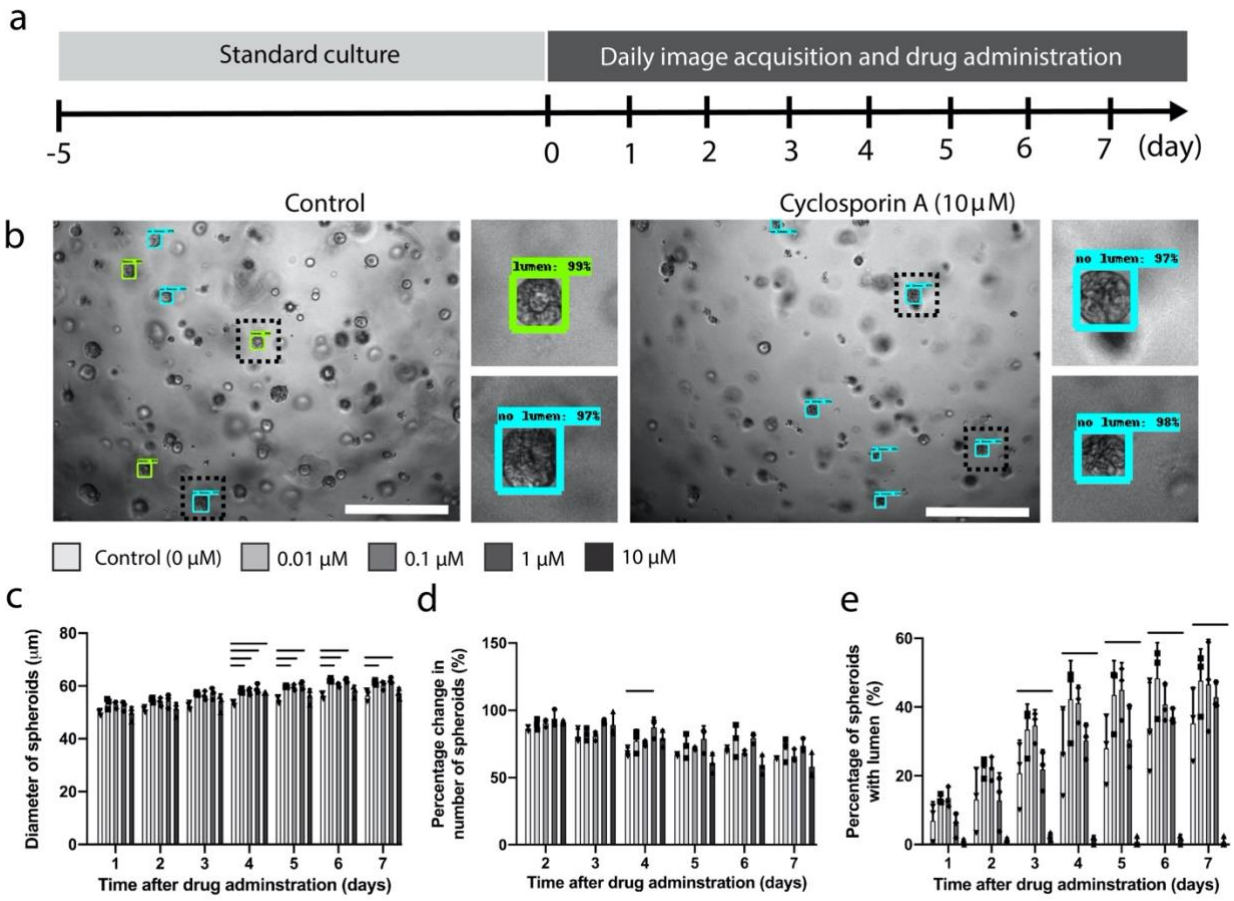

Figure 4. Validation of Deep-LUMEN with drug administration. a, Cyclosporin A administration timeline. Cyclosporin A was administered on the sixth day of lung spheroid culture for a period of seven days. **b**, Comparison of detections in control versus 10 μM drug-treated conditions. Deep-LUMEN was used to detect polarized and non-polarized spheroids following drug administration. Bright-field images were acquired by taking z-stack images of spheroids under 4X magnification (n = 3). Scale bar, 500 μm. **c,** Average diameter of spheroids following drug administration (n = 3). Bounding box coordinates of detections above a 50% score confidence were outputted to measure the diameter. Statistical significance was determined through a one-way ANOVA test followed by the Holm-Sidak method. Line indicates a p-value < 0.05. **d,** Percent change in the number of spheroids following a period of drug administration. Quantification was done by outputting detections that had at least a 50% score confidence. Statistical significance was determined through a two-way ANOVA test followed by the Holm-Sidak method. Line indicates a p-value < 0.05. **e,** Proportion of the lumen class of spheroids over the period of drug administration (n = 3). Quantification of lumen spheroids was obtained by filtering detections with at least a 50% score confidence that were of the lumen class. Statistical significance was determined through a one-way ANOVA test followed by the Holm-Sidak method. Line indicates a p-value < 0.05.

Table of contents

Deep-Learning Uncovered Measurement of Epithelial Networks (Deep-LUMEN) is an open-source object detection algorithm that has been fine-tuned to automatically uncover subtle differences in epithelial spheroid morphology from brightfield images. This algorithm can track changes in the luminal structure of 3D spheroids and distinguish between polarized and non-polarized lung epithelial spheroids. Deep-LUMEN could open new possibilities for assessing drug effects in 3D tissue models or be further expanded to conduct more complex phenotypic screens.

Keywords: Deep learning, Spheroids, Organoids, Organ-on-a-Chip, Drug screening

*Lyan Abdul[1], Shravanthi Rajasekar[2], Dawn S.Y Lin[2], Sibi Venkatasubramania Raja[3], Alexander Sotra[2], Yuhang Feng[3], Amy Liu[3] and Boyang Zhang[2,4]**

Title: Deep-LUMEN Assay – Human epithelial spheroid localization and classification using deep learning

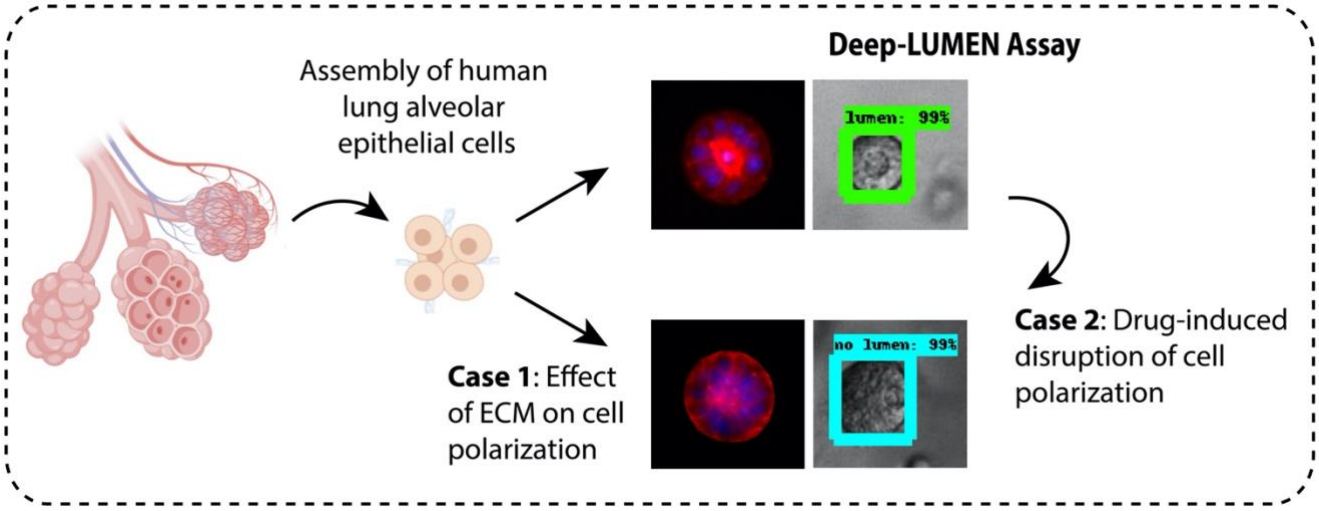

Supplementary Materials

Deep-LUMEN Assay – Human epithelial spheroid localization and classification using deep learning

Lyan Abdul[1], Shravanthi Rajasekar[2], Dawn S.Y. Lin[2], Sibi Venkatasubramania Raja[3], Alexander Sotra[2], Yuhang Feng[3], Amy Liu[3], and Boyang Zhang[2,4]*

[1]School of Interdisciplinary Science, McMaster University 1280 Main Street West, Hamilton, ON, L8S 4K1, Canada
[2]Department of Chemical Engineering, McMaster University, 1280 Main Street West, Hamilton, ON, L8S 4L8, Canada
[3]Faculty of Health Sciences, McMaster University 1280 Main Street West, Hamilton, ON, L8S 4L8, Canada
[4]School of Biomedical Engineering, McMaster University, 1280 Main Street West, Hamilton, ON, L8S 4L8, Canada

*Correspondence to zhangb97@mcmaster.ca

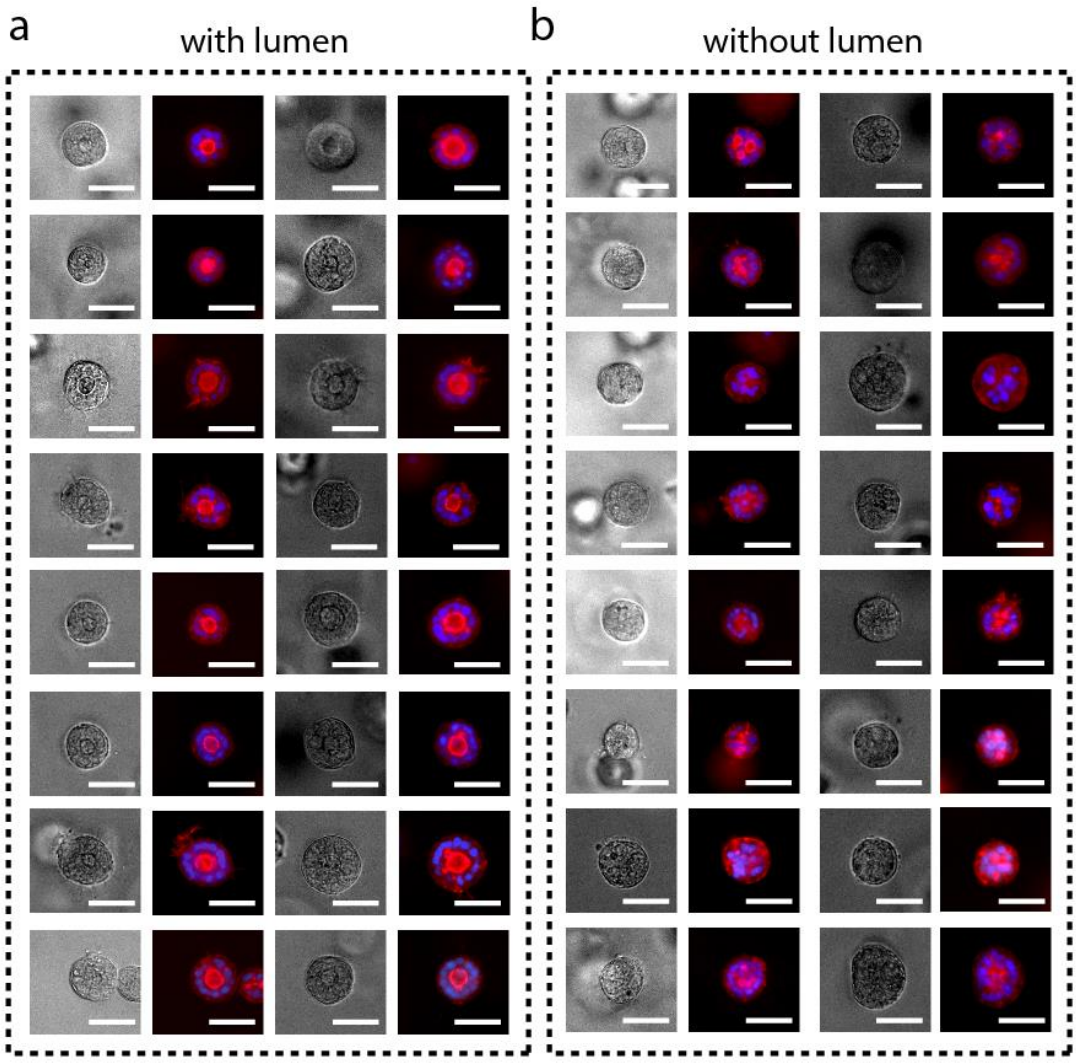

Supplementary Figure 1. Immunofluorescent staining of polarized and non-polarized lung spheroids. a-b, Fluorescent staining of (a) polarized spheroids referred to as "lumen" (representative images n = 6 samples) and (b) non-polarized spheroids referred to as "no lumen". Spheroids were stained for F-actin (red) and DAPI (blue). Scale bar, 50 μm.

Chapter 3: Application of deep learning to colon organoids

Organoids, which are derived from stem cells, develop into complex structures that mimic the structure and function of the native organ. First cultured in 2011, colon organoids exhibit key features of the colon epithelium *in vivo* including the expression of colon-specific cells and the crypt domains.[11] Colon organoids have been used to understand stem cell differentiation, drug toxicity, and colon pathophysiology. [23–26] However, deep learning-based methods to analyze colon organoids are minimal. In other organoid types, deep learning has been used to detect organoids, replace immunofluorescent stains, develop alternative cell viability assays, and for organoid segmentation.[15,16,27–29] However, colon organoid morphology hasn't been analyzed using deep learning techniques.

In this work, we developed D-CryptO, a tool to analyze the structural maturity of colon organoids directly from brightfield images. To do this, we created a new dataset for the morphologies of interest and used transfer learning techniques to train models with different architectures. Using the best-performing model, we validated it in several ways. We assessed (1) how colon organoid morphology changes over prolonged culture (2) how short-term forskolin stimulation affects organoid morphology and (3) how chemotherapeutic drugs disrupt organoid morphology. This work presents a second demonstration that deep learning can be used for 3D tissue morphology analysis. We also showed that despite having more complex and heterogeneous morphologies relative to spheroids, deep learning could detect structural changes. The validation studies also demonstrate that D-CryptO can be applied to analyze morphology in a broad set of cases. Finally, this work showed the significance of analyzing colon organoid morphology as we gained insights into potential mechanisms of drug-induced toxicity. Several authors contributed to this work and their contributions are outlined on page 47.

D-CryptO: Deep learning-based analysis of colon organoid morphology from brightfield images

Lyan Abdul, Jocelyn Xu, Alexander Sotra, Abbas Chaudary, Jerry Gao, Shravanthi Rajasekar, Nicky Anvari[1], Hamidreza Mahyar, and Boyang Zhang[*]

L.A., A.S., N.A., Dr. B.Z.
School of Biomedical Engineering, McMaster University, 1280 Main Street West, Hamilton, ON, L8S 4L8, Canada

E-mail: zhangb97@mcmaster.ca

J.X.
Faculty of Engineering, McMaster University, 1280 Main Street West, Hamilton, ON, L8S 4L8, Canada

A.C., S.R., Dr. B.Z.
Department of Chemical Engineering, McMaster University, 1280 Main Street West, Hamilton, ON, L8S 4L8, Canada

J.G.
Faculty of Science, McGill University, 845 Sherbrooke Street West, Montreal, QC H3A 0G4, Canada

Dr. H.M.
W Booth School of Engineering Practice and Technology, McMaster University, 1280 Main Street West, Hamilton, ON, L8S 4L8, Canada

Keywords: deep learning, image analysis, organoids, morphology, drug testing, brightfield images

Stem cell-derived organoids are a promising tool to model native human tissues as they resemble human organs functionally and structurally compared to traditional monolayer cell-based assays. For instance, colon organoids can spontaneously develop crypt-like structures similar to those found in the native colon. While analyzing the structural development of organoids can be a valuable readout, using traditional image analysis tools makes it challenging because of the heterogeneities and the abstract nature in organoid morphologies. To address this limitation, we developed and validated a deep learning-based image analysis

tool, named D-CryptO, for the classification of organoid morphology. D-CryptO can automatically assess the crypt formation and opacity of colorectal organoids from brightfield images to determine the extent of organoid structural maturity. To validate this tool, changes in organoid morphology were analyzed over long-term organoid passaging and short-term forskolin stimulation. To further demonstrate the potential of D-CryptO for drug testing, organoid structures were analyzed following treatments with a panel of chemotherapeutic drugs. With D-CryptO, subtle variations in how colon organoids responded to the different chemotherapeutic drugs were detected, which suggest potentially distinct mechanisms of action. This tool could be expanded to other organoid types, like intestinal organoids, to facilitate 3D tissue morphological analysis.

1. Introduction

Monolayer cell-based assays are an invaluable tool for studying cellular functions *in vitro*. However, these models do not accurately recapitulate *in vivo* tissue responses. This is largely because monolayer cell models do not exhibit tissue-specific architecture and lack the appropriate 3D cellular microenvironment. Stem cell-derived organoids that can spontaneously differentiate and self-assemble into 3D tissues with structures that resemble many features of the native organ have emerged as alternative *in vitro* models.[1] For instance, colon organoids have been widely used as large intestine models due to their structural and functional similarity. [2] An important feature of the colon epithelium is the crypt, which are epithelial invaginations that renew the intestinal lining every 3-5 days. [3] The organization of the crypt is crucial for the regeneration of the epithelium *in vivo*. Stem cells at the base of the crypt are protected from continuous mechanical and chemical stressors, and as a result, can proliferate and differentiate to regenerate the epithelium. Similarly, colon organoid morphology reflects the structure and organization of the native colon crypts by exhibiting

budding structures which contain the stem cells that give rise to colon-specific cells. [4,5] Therefore, analyzing organoid morphology can provide insights into colon physiology and pathophysiology in vivo.

Qualitative analysis of colon organoid morphology, specifically the opacity and budding of organoids has largely been used to assess the maturity of colon organoids. Colon organoids that are more transparent, have thinner walls, and are cystic are indicative of an earlier differentiation state.[6] On the other hand, colon organoids have reached a more differentiated state when they are more opaque due to the thickening of the epithelial wall. Differentiated colon organoids also exhibit more budding structures that resemble the colon crypt which is the stem cell niche that controls colonocyte renewal and homeostasis.[2] Previously, the presence of budding within small intestinal organoids has been used to optimize the extracellular matrix, to study stem cell differentiation, and to understand the mechanics of epithelial folding. [3,7–9] Analysis of budding has also been used to study diseases. For example, colon organoids from individuals with inflammatory bowel disease or tumour-derived organoids had lower rates of budding structures.[10,11] However, to assess these morphological differences, previous work used manual analysis or relied on traditional image analysis that use imperfect parameters such as eccentricity to describe organoid shapes.[12–14]

To facilitate the morphological analysis of organoids with abstract features that are not easily defined by traditional image analysis parameters, a type of computer vision called deep learning can be applied. Deep learning refers to an automated method of computer-based image recognition that relies on using pre-existing data to make predictions on new image instances.[15] Traditional computer recognition techniques rely on manual feature extraction to distinguish between the categories of interest. With deep neural networks, both feature extraction and classification are done automatically without any input from the user. This

provides several advantages. First, colon organoid features are learned directly from the images without the need for manual feature extraction. Second, analysis of the structures is not limited to using shape descriptors, so organoid morphology can be characterized despite the high heterogeneity of colon organoid structure. Third, automatic image analysis can improve the throughput of morphological analysis. Finally, these models could be trained to correctly classify between categories despite imaging artifacts. Artificial neural networks have been previously used to detect and count intestinal organoids and replace immunostaining and cell viability assays. [16–19] However, deep learning has yet to be applied for the morphological characterization of any type of organoids.

Hence, we used deep learning to characterize the morphological structure of organoids by developing an analysis tool, D-CryptO, to classify between transparent and opaque organoids, as well as spherical and budding organoids. Collectively, these features reveal the structural maturity and health of colon organoids. To validate our deep learning model, we analyzed changes in colon organoid morphologies in (1) long-term organoid passaging, (2) short-term forskolin stimulation, (3) a drug screening study with a panel of six chemotherapeutic drugs, and (4) a dose response study to doxorubicin. We found that morphological analysis allowed us to capture variations in how colon organoids responded to the different chemotherapeutic drugs, which provide insights into the potential mechanisms of drug toxicity.

2. Results

2.1. Colon organoid culture and morphological characteristics

Colorectal organoids, derived from primary colon tissue, were embedded in Matrigel, and cultured for a period of 7 days in a 24-well plate **(Figure 1a-b)**. The primary tissue contains adult stem cells which proliferate and differentiate to form the colon organoids *in vitro*. We

observed a spectrum of morphologies from these colon organoids. Organoids differed in their opacity as well as the extent of budding **(Figure 1c)**. Colonospheres are transparent with little-to-no budding. On the other hand, colonoids are more mature organoids that are opaque with significant number of budding structures.[20,21] As the proliferating stem cells differentiate into organ-specific cells, opacity increases due to changes in epithelium thickness. [7] We also observed organoids that exhibited some characteristics of both colonospheres and colonoids. For example, some organoids were spherical and opaque while other organoids had buds and were transparent. Hence, using the parameters of both opacity and budding could give an indication of the structural maturity of the organoids grown *in vitro.*

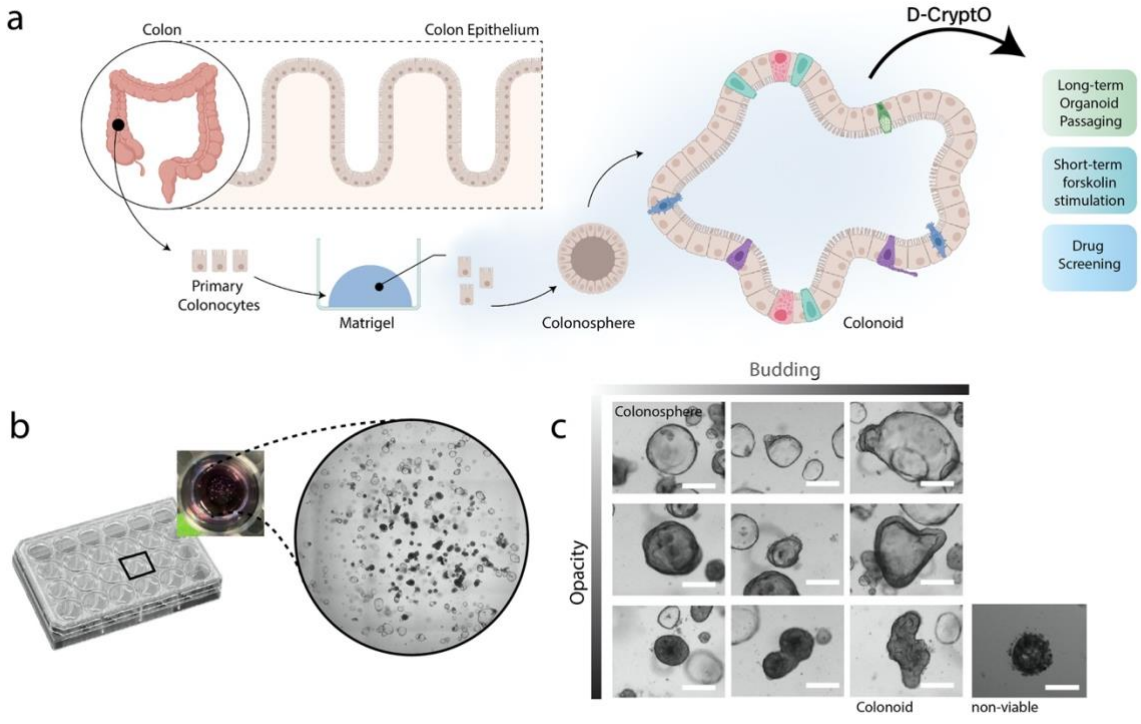

Figure 1. Morphological heterogeneity of colon organoids. a, Illustration of primary cells embedded in Matrigel® that self-assemble into colonospheres and develop into colonoids. **b,** Organoids embedded in 50µL of Matrigel® in a standard 24-well plate. **c,** Representative images of organoids exhibiting varying levels of opacity and budding. Scale bar, 200 µm

2.2 Dataset creation and model training

To analyze these parameters using deep learning, we first created two custom datasets using images of individual organoids. The first dataset consisted of examples of budding and spherical organoids. The second dataset contained examples of opaque and transparent organoids **(Figure 2a)**. The dataset for opacity contained 1021 images of opaque organoids and 1457 images of transparent organoids. The dataset for the budding feature contained 1081 images of budding organoids and 1395 images of non-budding organoids. These datasets were further split into training, validation, and test datasets. We made the full training dataset publicly accessible at the open science framework data repository: https://osf.io/42r3g/. Next, we fine-tuned six pre-trained deep neural network models (ResNet152V2, XCeption, InceptionResNetV2, VGG-16, VGG-19, ResNet50) for each parameter using the custom datasets.[22–26] These models were selected either because they had higher speeds or performed more accurately on the ImageNet dataset. We implemented these transfer learning approaches using the Keras framework with the Tensorflow backend.[27] For opacity, both XCeption and VGG-16 performed with an accuracy of 98% on the test set. For budding, both ResNet152V2 and XCeption performed with an accuracy of 90.87% on the test set. XCeption, a convolutional neural network model, was chosen as the final model since it performed most accurately for both parameters **(Figure 2b)**. To understand which regions of the organoid were used for classification, heat maps were outputted to highlight important locations **(Figure 2c)**. For the opacity model, the center of the organoid is important for distinguishing between opaque and transparent organoids. For the budding model, the edges of the organoids are used to distinguish between budding and spherical organoids. For opacity, there was a lower rate of false positives and negatives compared to budding **(Figure 2d, e)**. This could be due to the lower heterogeneity in the opacity of organoids compared to the budding morphologies. Nonetheless, accuracy was above 85% for both parameters and both models

had low rates of false negatives. Together, these trained models were combined to become D-CryptO for analyzing colon organoid morphology and determine the extent of colon organoid maturation. Lastly, we showed D-CryptO can successfully capture the extent of differences in morphology in both budding and opacity characteristics, with a prediction score that reflects where the organoid falls on the spectrum of budding or opacity **(Figure 2f, g)**.

a

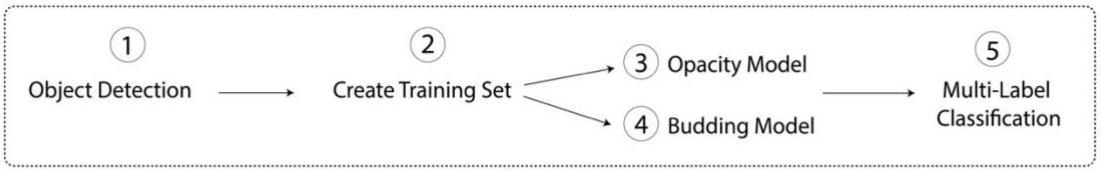

b

Model Name	Number	Opacity Accuracy	Budding Accuracy
ResNet152V2	1	97.60%	90.87%
XCeption	2	98.00%	90.87%
InceptionResNetV2	3	96.80%	87.3%
VGG-16	4	98.00%	89.29%
VGG-19	5	97.20%	88.49%
ResNet50	6	97.20%	89.68%

c

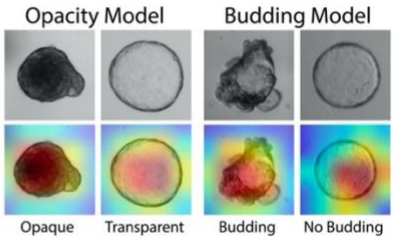

d

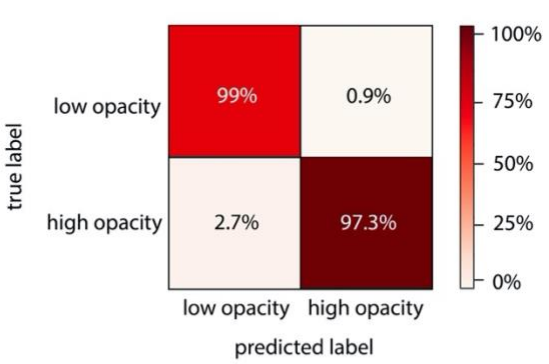

e

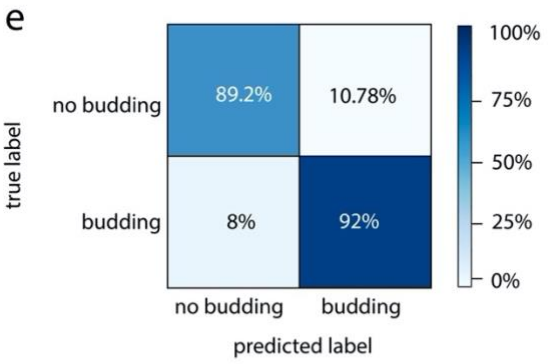

f

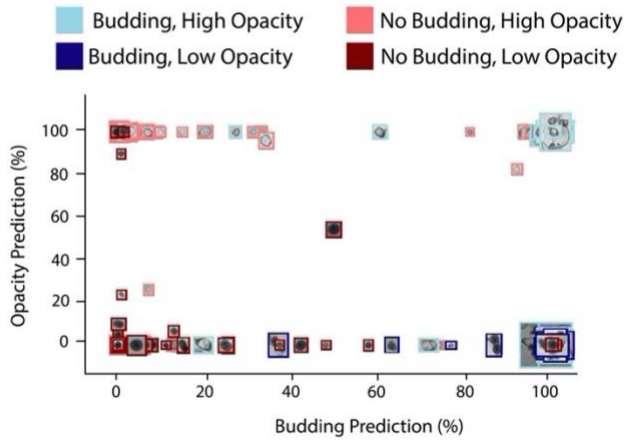

g

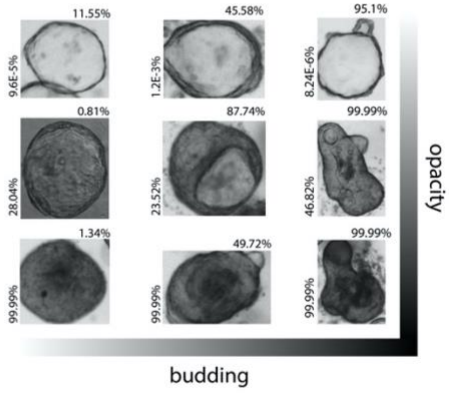

Figure 2. D-CryptO training and testing. a, Image analysis workflow. **b,** Accuracy of trained models on test set following transfer learning. **c,** Heatmaps identifying which parts of the image were more important for organoid classification (red indicate higher importance and blue indicate lower importance). **d,** Confusion matrix for the opacity feature of D-CryptO. **e,** Confusion matrix for the budding feature of D-CryptO. **f,** Organoid distribution based on D-CryptO predictions for opacity and budding. **g,** Representative D-CryptO organoid classification prediction score and corresponding brightfield images.

2.3 Morphological changes of organoids over long term organoid expansion and passaging

To validate D-CryptO, we used it to analyze organoid morphology in a number of different case studies. While colon organoids are a valuable tool for biological applications, there is a lot of variability in morphology within a single Matrigel dome. This can hinder reproducibility of experimental results over long-term culture. We analyzed opacity and budding to determine variability in morphology over prolonged culture **(Figure 3a,b)**. First, we analyzed organoids after thawing them directly into a 24-well plate and culturing them for 5 days. The average percentage of opaque organoids was 21.4 ± 2.9% while the average percentage of budding organoids was 74.5% ± 2.1%. Average organoid diameter was 271.4 μm ± 14.4 μm. Next, we passaged the organoids and repeated the analysis. While there was greater variability in different wells, there wasn't a significant difference in opacity, budding and diameter following passaging **(Figure 3c,d,e)**. This demonstrates that organoids remain robust following one passage, but further analysis is required to see how a greater number of passages impacts organoid morphology. Nonetheless, D-CryptO could be used to analyze colon organoid culture to assess organoid morphology over time non-invasively.

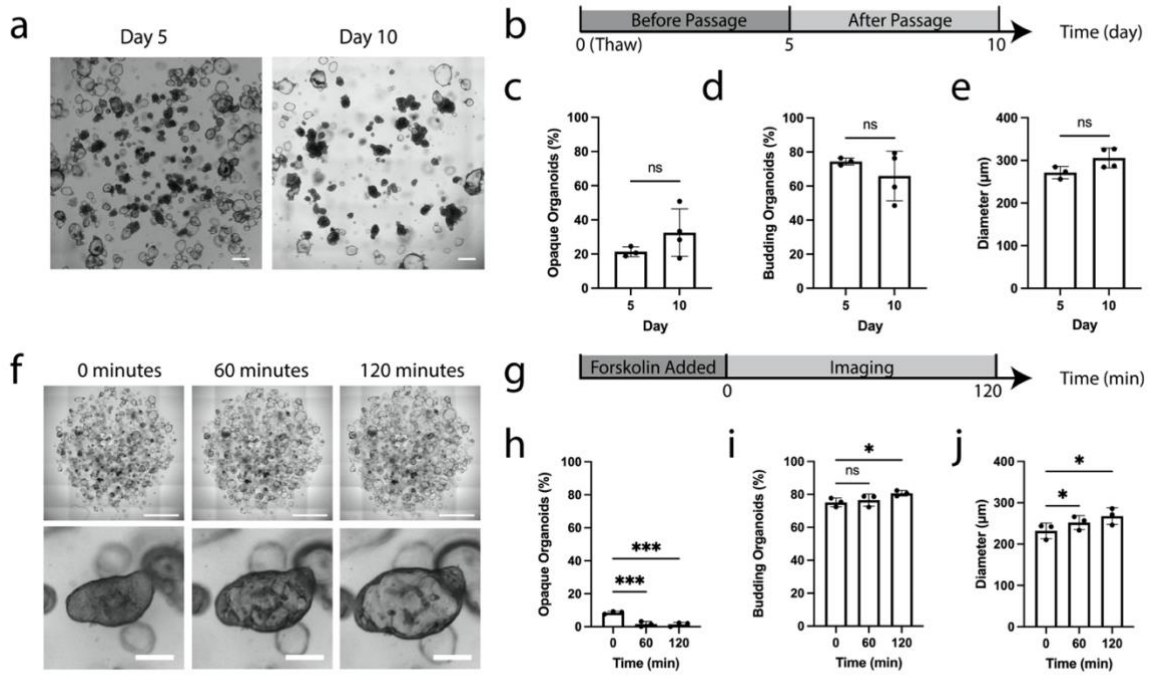

Figure 3. Organoid morphological changes over long-term passaging and short-term forskolin stimulation. a, Brightfield images of organoids cultured over two weeks. Scale bar, 500 µm. **b,** Timeline of organoid culture. Organoids were thawed and cultured for 1 week and were subsequently passaged. **c-e,** Quantification of the percentage of opaque organoids, percentage of budding organoids and diameter of organoids (n=3-4) on day 5 and 10. **f,** Brightfield images of organoids during forskolin stimulation. Scale bar (top), 2000 µm. Scale bar (bottom), 100 µm. **g,** Timeline of forskolin treatment. **h-j,** Quantification of the percentage of opaque organoids, budding organoids, and diameter of organoids following 60 and 120 minutes of forskolin treatment (n=3). *p < 0.05, **p < 0.01, ***p < 0.001.

2.4 Morphological changes of organoids to short term exposure of external stimuli

Next, we used D-CryptO to assess changes in organoid morphology during short-term perturbation. Colon organoids were thawed and embedded in Matrigel in a 24-well plate and cultured for a period for 10 days. We applied 10 µM of forskolin, a small molecule that activates the cystic fibrosis transmembrane conductance regulator (CFTR), for a period of 2 hours **(Figure 3f,g)**. The CFTR channel is essential for ion transport and mucus production in the colon. In healthy organoids that have a functional CFTR channel, forskolin treatment results in the opening of the channel, the movement of chloride ions through the CFTR

channel, and the subsequent flux of water into the organoid. As a result, the organoid swells. However, forskolin treatment in organoids with mutations in the CFTR channel do not exhibit this response.[28] Using D-CryptO, we analyzed changes in opacity and budding in response to forskolin. The percentage of opaque organoids significantly decreased following 60 and 120 minutes of forskolin treatment since water was accumulating within the organoid lumen **(Figure 3h)**. Budding also increased slightly after 120 minutes (**Figure 3i**). This could be due to the budding domains of the organoids becoming more apparent following forskolin stimulation. Diameter also increased following forskolin stimulation, as expected due to organoid swelling **(Figure 3j)**.

2.5 Morphological changes of organoids in response to drug treatments

Chemotherapeutic drugs have been shown to induce gastrointestinal toxicity *in vivo* which can affect treatment outcomes.[29] We used D-CryptO to assess the effect of different clinically approved chemotherapeutics at a single dosage on colon organoid morphology. We thawed colon organoids directly into a 384-well plate and applied 6 chemotherapeutic drugs at a concentration of 50 µM to the organoids following 4 and 10 days of culture **(Figure 4a)**. This concentration is higher than maximum recommended plasma clinical concentrations or has been previously shown to have toxic effects in colon organoids.[29,30] WHEN comparing the docetaxel and cisplatin-treated organoids to the control, there wasn't any significant difference in the percentage of opaque and budding organoids or in the diameter of the organoids, which is an indication that these drugs did not have a toxic effect at this concentration **(Figure 4d,f)**. Under fluorouracil treatment, opacity and budding of organoids was not affected, but the diameter was significantly decreased **(Figure 4e)**. This could indicate that fluorouracil inhibited organoid growth. This similar morphological change and effect was also seen in the organoids treated with chlorambucil **(Figure 4i)**. Organoids treated with erlotinib exhibited different effects. The percentage of opaque organoids increased, the

percentage of budding organoids decreased, and the diameter decreased **(Figure 4g)**. This could indicate that erlotinib prevented stem cell proliferation and differentiation, which affected organoid assembly. Doxorubicin treatment resulted in a significantly higher percentage of opaque and budding organoids, and organoid diameter decreased **(Figure 4h)**. When examining the images, it was more apparent that budding did not actually increase, but that there was a higher percentage of non-viable and dissociating organoids, which were falsely classified as organoids containing budding features. This morphological change could indicate that doxorubicin induced toxicity in colon organoids and triggered cell apoptosis. Therefore, by analyzing all three organoid morphological parameters, budding, opacity and diameter holistically, we can gain new insights into the potential mechanisms of drug-induced toxicity.

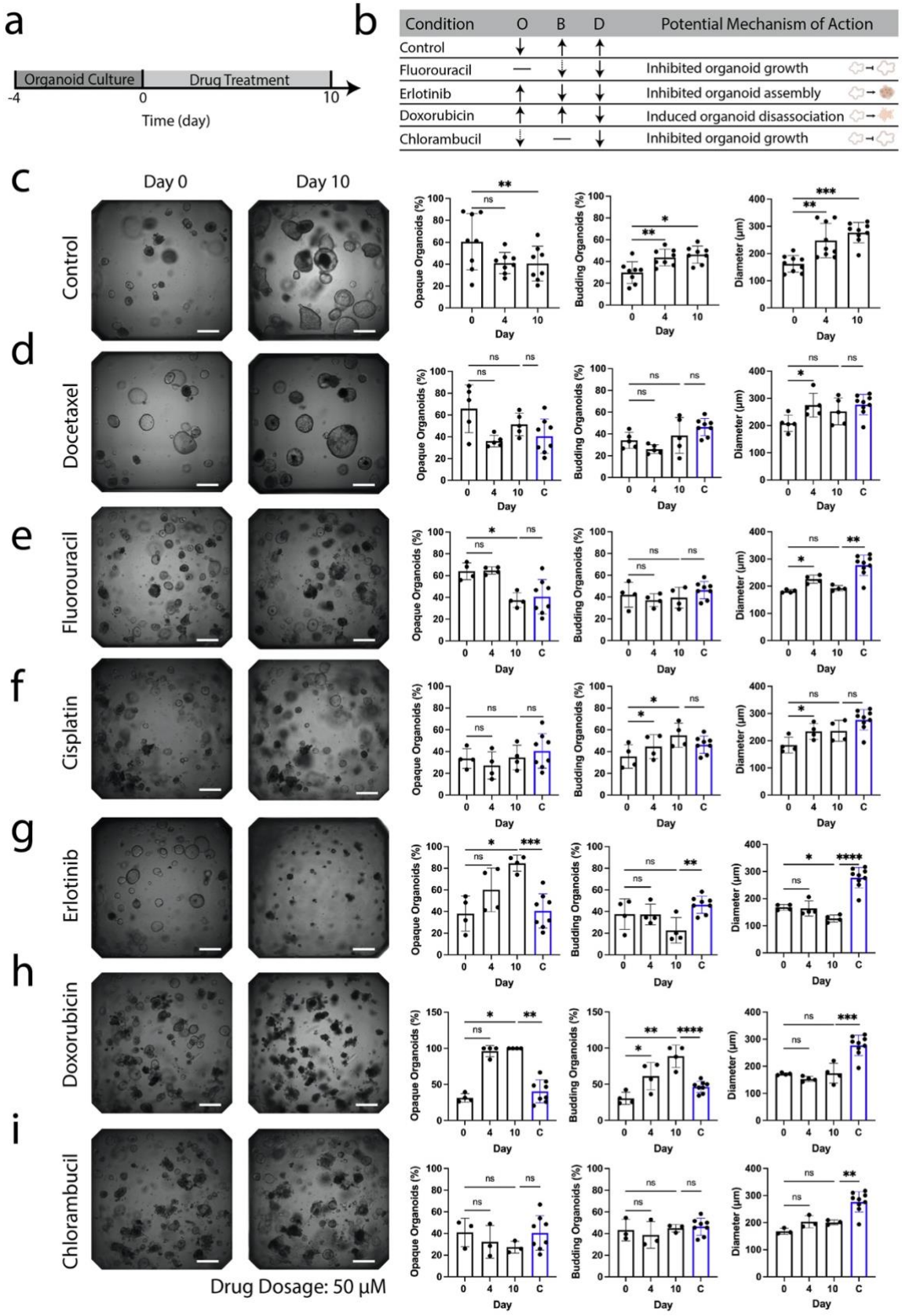

Figure 4. Chemotherapeutic drug-induced morphological changes in organoids. a, Timeline of organoid culture and drug treatment. **b,** An outline of drug-induced effects on organoid opacity (O), budding (B), diameter (D), and potential mechanisms of action. Arrows

with dashed lines indicate a non-significant difference compared to day 10 control. **c,** Brightfield images of organoids in the non-treated condition and quantification of the changes in opacity, budding, and diameter of organoids following 10 days of culture (n=4). **d-i,** Organoid brightfield images (4× magnification) and quantification of the changes in opacity, budding, and diameter on days 0, 4, and 10 and comparison of day 10 values to the day 10 no treatment control values (C) following treatment with **(d)** docetaxel (n=4), **(e)** fluorouracil (n=4), **(f)** cisplatin (n=4), **(g)** erlotinib (n=4), **(h)** doxorubicin (n=4), and **(i)** chlorambucil (n=3). Scale bar, 500 μm. *p < 0.05, **p < 0.01, ***p < 0.001, ****p < 0.0001.

3. Discussion

Analyzing the structural complexity within organoids can provide valuable insights.

So far deep learning methods have mainly been used to detect, segment or track organoids.[12,17] We developed a deep-learning based method, D-CryptO, to characterize the complex structural morphology of organoids for the first time. As a result, the extent of organoid maturity can be analyzed automatically without the use of invasive analyses such as immunofluorescent staining. We validated this tool by analyzing changes in organoid morphology in prolonged culture, in short-term perturbation with forskolin, and in chemotherapeutic drug screening to assess drug toxicity. D-CryptO provides a number of advantages over existing organoid analysis workflows. First, despite the high inter-organoid heterogeneity, D-CryptO accurately categorized organoid opacity and budding. Second, D-CryptO uses brightfield images that allows for non-destructive organoid analysis. Lastly, since D-CryptO makes classifications on single organoids, image analysis can easily be done on organoids grown in a 24-well plate or be scaled up to a 384-well plate as we have shown. D-CryptO can also be further expanded to monitor each organoid's development overtime at single organoid resolution as they transition from colonospheres to colonoids.[12,31]

Despite the advantages of D-CryptO, there are some limitations. First, organoids treated with cytotoxic compounds were identified as having increased budding structures. This is possibly due to cell death aggregations having a similar morphological outline to budding organoids. To address this, D-CryptO can be specifically trained to identify non-viable and dissociating

organoids. Furthermore, blurry organoids or overlapping organoids, although part of the training dataset, were occasionally misclassified. The training dataset could be increased to improve classification accuracy. Finally, D-CryptO was specifically trained to assess crypt structures of colon organoids, but it is unclear whether D-CryptO can be applied to organoids from other organoids like the small intestine. While many other types of organoids do also exhibit budding features, more transfer learning might be needed for morphological assessment of other types of organoids.[32]

4. Conclusion

Colon organoid morphology exhibits key features of the colon epithelium *in vivo* and could provide information on colon physiology and pathophysiology. In this work, we developed D-CryptO, a deep learning tool to automatically analyze colon organoid structure. Specifically, D-CryptO can analyze the opacity and the presence of budding within colon organoids to assess the extent of tissue maturation and differentiation. To validate D-CryptO, we used it to analyze colon organoid morphology in several cases. We analyzed changes in organoid morphology over long-term organoid culture, during short-term exposure to forskolin, and in a drug screen with a panel of chemotherapeutic drugs. By using D-CryptO to analyze organoid structure following drug treatment, we gained insights into the potential mechanisms by which the drugs induced toxic effects. D-CryptO can help facilitate the analysis of colon organoid morphology to better understand tissue physiology *in vivo*, assess drug effects, and develop therapies.

5. Methods

Colon organoid culture: Patient-derived colorectal organoids were acquired from the University Health Network (UHN) Princess Margaret Living Biobank in Toronto Canada.

Approval for the use of these organoids were obtained from the Hamilton Integrated Research Ethics Board under the project number, 5982-T. Organoids were derived from a 69-year-old, female patient. Organoids were cultured by thawing frozen vials and embedding them into growth-factor reduced Matrigel. 50µL of Matrigel and the organoids were casted into a 24-well plate. Organoids were maintained using Intesticult human organoid growth media purchased from Stemcell Technologies (Cat #06010) supplemented with Rock Inhibitor. For experiments in a 384-well plate, organoids were thawed directly and embedded in 25µL of Matrigel. Organoids used in these experiments were between passage 18-19.

Image acquisition: Brightfield images of colorectal organoids were acquired using a Cytation 5 cell imaging multi-mode reader (BioTek® Instruments). Both image montages and z-stacks were captured at 4×magnification. Acquired images were then converted into the png and rgb format.

Dataset creation: A set of image montages composed of 35 images were obtained from organoids cultured in a 24-well plate. Each organoid within the image was labelled using labelImg, and its coordinates were used to automatically crop each organoid. Organoids were then sorted into separate datasets. For the opacity dataset, if the organoid had a thin epithelium, or a clear lumen it was classified as transparent. If the organoid had a thicker epithelium or did not have a clear lumen, it was classified as opaque. The opacity training dataset consisted of 816 opaque organoids and 1165 transparent organoids. The opacity validation dataset consisted of 101 opaque organoids and 144 transparent organoids. The opacity test dataset contained 104 opaque organoids and 148 transparent organoids. Images were randomly split into the datasets with a ratio of 80:10:10. For the budding dataset, if an organoid had a clear protrusion it was classified as a budding organoid. If an organoid was

mainly spherical, it was classified as non-budding. The budding training dataset contained 979 images of budding organoids and 1245 images of non-budding organoids. The budding test set had 102 images of budding organoids and 150 images of non-budding organoids. The budding validation set was created automatically using Keras with a validation split of 20%. The raw data set can be found at https://osf.io/42r3g/.

Model architecture and selection: Six pre-trained models were selected for transfer learning: ResNet152V2, XCeption, InceptionResNetV2, VGG-16, VGG-19, and ResNet50. These models were selected based on their performance on the ImageNet dataset as well as their speed. Additionally, these models have different architectures. VGG-16 contains 16 layers, consisting of convolutional layers and max-pooling layers, followed by a densely connected classifier. VGG19 has a similar architecture but consists of 19 layers. ResNet50 contains 50 layers and uses residual connections to reduce the problem of vanishing gradients and improve accuracy. ResNet152V2 also incorporates residual connections but is a deeper model with 152 layers. XCeption uses depthwise separable convolutions to generate a model with fewer parameters and increase performance. InceptionResNetV2 contains 164 layers and combines the Inception architecture, which includes different convolutional filter sizes and incorporates the residual connections of the ResNet architecture.

Model configuration and training: Keras (version 2.8.0) and python 3.7 was used to configure and train all models. First, all images were preprocessed into a tf.data.Dataset. Image size for all models was set to (150 pixels, 150 pixels), the batch size was set to 32 and image pixels were normalized to values between 1 and -1. For the opacity feature of D-CryptO, both feature extraction and fine-tuning were conducted. To do this, each of the 6 models with different architectures (ResNet152V2, XCeption, InceptionResNetV2, VGG-16, VGG-19, and ResNet50) were first instantiated and the pre-trained weights were loaded into them. All

layers in the pretrained models were frozen and a new classifier was added which included a dropout layer (dropout rate of 0.2) and a dense layer with 2 nodes and the softmax activation function. The model was then trained for 20 epochs using the Adam optimizer, the categorical cross entropy loss function, and the categorical accuracy metric to assess model performance. To further improve model performance for opacity, the models were fine-tuned by unfreezing all layers and the model was retrained at a low learning rate of 1×10^{-5} for 10 epochs with the same loss function and accuracy metric used for feature extraction. For the budding feature of D-CryptO, only feature extraction as described earlier was performed. All budding models were trained for 20 epochs and model performance was monitored using the precision metric. All training was done using GPU accessed through Google Colab. Data augmentation was used in all training pipelines to improve model performance by increasing the dataset available to train the model and reducing overfitting. The following data augmentation functions were applied: random flip, random rotation, and random zoom.

Forskolin treatment: Forskolin was purchased from STEMCELL Technologies (Cat# 72112). A stock solution of 10mM was prepared following manufacturer instructions. The 10mM stock solution was diluted to 10µM in 1×PBS (Cat#: 14190144). Colorectal organoids were cultured in a 24-well plate for a period of 7-10 days. Forskolin was administered for a period of 2 hours. Brightfield montage images at 4× magnification were taken every 15 minutes using the Cytation 5 cell imaging-multi mode reader.

Chemotherapeutic drug screen: Drugs were acquired from the NIH National Cancer Institute at stock concentration of 10mM diluted in DMSO. Drugs were diluted 200× in Intesticult Medium to achieve a concentration of 50µM. Colon organoids were thawed and embedded in 25µL of Matrigel in a 384 well plate. Following 4 days of culture, drugs were applied. Drug

solutions were renewed every other day. Z-stack montages were acquired every other day using a Cytation 5 cell imaging-multi mode reader.

Quantification analysis: Individual organoids within image montages were detected using OrgaQuant[17] or had boxes drawn around them manually using the SuperAnnotate software. To assess changes in budding and opacity, all predictions by the final trained models were outputted to a CSV file. For opacity, any organoids which had classification score of greater than 50% was classified as opaque. For budding, any organoids which had a classification score of greater than 50% was classified as budding. The change in budding and opacity was assessed in at least 3 independent samples. To measure diameter, the x coordinates from the bounding boxes of the detected organoids were used. Diameter was obtained from at least 3 independent samples. Confusion matrices and the organoid distribution dot plot were plotted using the Matplotlib library.

Statistical analysis: All results are plotted as mean ± standard deviation. Normality and equal variance were tested for using GraphPad. A p value < 0.05 was considered statistically significant in all experiments. At least three independent samples were used for all experiments. For data in **Figures 3h-j**, statistical significance was determined using a one-way repeated measurement ANOVA followed by Dunnett's test. Statistical significance for **Figures 3c-e** was assessed using an unpaired two-tailed t-test. For Figure 4, statistical significance was assessed using a one-way repeated measurement ANOVA followed by Dunnett's test. Statistical significance for changes in diameter following treatment with Erlotinib (Figure 4g) and the changes in opacity in the organoids treated with doxorubicin (Figure 4h) were assessed using the Friedman test followed by Dunn's test. Statistical significance between day 10 opacity, budding, and diameter values to day 10 control values was determined using a two-tailed unpaired t-test. Statistical significance in the opacity of the

organoids to the day 10 control in the organoids treated with doxorubicin was assessed using the Mann-Whitney test.

Data availability

All the trained models and the datasets can be downloaded from: https://osf.io/42r3g/

Supporting Information

Supporting Information is available from the Wiley Online Library or from the author.

Acknowledgements

This work was funded by the National Sciences and Engineering Research Council of Canada (NSERC) Discovery Grant (RGPIN-05500-2018), and Canadian Institute of Health Research (CIHR) Project Grant (PJT-166052) to BZ. This work was made possible by the financial support of Canada Graduate Scholarship to L.A. The authors are grateful to BioRender.com which we have used to make the illustrations in this work.

Author contribution

L.A. performed the experiments, deep learning analysis, and prepared the manuscript. J.X. helped with dataset creation and model training. A.S. contributed to the culturing of colon organoids. A.C. and J.G. contributed to the dataset creation. S.R. contributed to colon organoid culture. N.A. and H.M. reviewed and edited the manuscript. B.Z. envisioned the concept, supervised the work and edited the manuscript.

Competing financial interests

None.

Received: ((will be filled in by the editorial staff))
Revised: ((will be filled in by the editorial staff))
Published online: ((will be filled in by the editorial staff))

References

1. Jensen, C. & Teng, Y. Is It Time to Start Transitioning From 2D to 3D Cell Culture? *Frontiers in Molecular Biosciences* **7**, 33 (2020).
2. Kola, I. & Landis, J. Can the pharmaceutical industry reduce attrition rates? *Nature Reviews Drug Discovery 2004 3:8* **3**, 711–716 (2004).
3. Torras, N., García-Díaz, M., Fernández-Majada, V. & Martínez, E. Mimicking epithelial tissues in three-dimensional cell culture models. *Frontiers in Bioengineering and Biotechnology* **6**, 197 (2018).
4. Ramaiahgari, S. C. *et al.* A 3D in vitro model of differentiated HepG2 cell spheroids with improved liver-like properties for repeated dose high-throughput toxicity studies. *Arch Toxicol* **88**, 1083–1095 (2014).
5. Mizuguchi, K. *et al.* Three-dimensional spheroid culture induces apical-basal polarity and the original characteristics of immortalized human renal proximal tubule epithelial cells. *Exp Cell Res* **404**, (2021).
6. Co, J. Y. *et al.* Controlling Epithelial Polarity: A Human Enteroid Model for Host-Pathogen Interactions. *Cell Reports* **26**, (2019).
7. Giles, R. H., Ajzenberg, H. & Jackson, P. K. 3D spheroid model of mIMCD3 cells for studying ciliopathies and renal epithelial disorders. *Nat Protoc* **9**, 2725–2731 (2014).
8. Kim, J., Koo, B. K. & Knoblich, J. A. Human organoids: model systems for human biology and medicine. *Nature Reviews Molecular Cell Biology 2020 21:10* **21**, 571–584 (2020).
9. Morizane, R. *et al.* Nephron organoids derived from human pluripotent stem cells model kidney development and injury. *Nat Biotechnol* **33**, 1193–1200 (2015).
10. Lancaster, M. A. *et al.* Cerebral organoids model human brain development and microcephaly. *Nature* **501**, 373–379 (2013).
11. Sato, T. *et al.* Long-term Expansion of Epithelial Organoids From Human Colon, Adenoma, Adenocarcinoma, and Barrett's Epithelium. *Gastroenterology* **141**, 1762–1772 (2011).
12. Sato, T. *et al.* Single Lgr5 stem cells build crypt-villus structures in vitro without a mesenchymal niche. *Nature 2009 459:7244* **459**, 262–265 (2009).
13. Shamir, L., Delaney, J. D., Orlov, N., Eckley, D. M. & Goldberg, I. G. Pattern Recognition Software and Techniques for Biological Image Analysis. *PLOS Computational Biology* **6**, e1000974 (2010).
14. Lecun, Y., Bengio, Y. & Hinton, G. Deep learning. *Nature 2015 521:7553* **521**, 436–444 (2015).
15. Kassis, T., Hernandez-Gordillo, V., Langer, R. & Griffith, L. G. OrgaQuant: Human Intestinal Organoid Localization and Quantification Using Deep Convolutional Neural Networks. *Scientific Reports 2019 9:1* **9**, 1–7 (2019).

16. Kegeles, E., Naumov, A., Karpulevich, E. A., Volchkov, P. & Baranov, P. Convolutional Neural Networks Can Predict Retinal Differentiation in Retinal Organoids. *Frontiers in Cellular Neuroscience* **14**, 171 (2020).
17. Lacalle, D. *et al.* SpheroidJ: An Open-Source Set of Tools for Spheroid Segmentation. *Comput Methods Programs Biomed* **200**, (2021).
18. Okuyama, H. *et al.* Dynamic Change of Polarity in Primary Cultured Spheroids of Human Colorectal Adenocarcinoma and Its Role in Metastasis. *The American Journal of Pathology* **186**, 899–911 (2016).
19. Vasquez, C. G., Vachharajani, V. T., Garzon-Coral, C. & Dunn, A. R. Physical basis for the determination of lumen shape in a simple epithelium. *Nat Commun* **12**, (2021).
20. Soetje, B., Fuellekrug, J., Haffner, D. & Ziegler, W. H. Application and Comparison of Supervised Learning Strategies to Classify Polarity of Epithelial Cell Spheroids in 3D Culture. *Frontiers in Genetics* **11**, 248 (2020).
21. Benning, L., Peintner, A., Finkenzeller, G. & Peintner, L. Automated spheroid generation, drug application and efficacy screening using a deep learning classification: a feasibility study. *Scientific Reports* **10**, 11071 (2020).
22. Abdul, L. *et al.* Deep-LUMEN assay – human lung epithelial spheroid classification from brightfield images using deep learning. *Lab on a Chip* **20**, 4623–4631 (2020).
23. Múnera, J. O. *et al.* Differentiation of Human Pluripotent Stem Cells into Colonic Organoids via Transient Activation of BMP Signaling. *Cell Stem Cell* **21**, 51-64.e6 (2017).
24. Crespo, M. *et al.* Colonic organoids derived from human induced pluripotent stem cells for modeling colorectal cancer and drug testing. *Nature Medicine 2017 23:7* **23**, 878–884 (2017).
25. Rodrigues, D. *et al.* New insights into the mechanisms underlying 5-fluorouracil-induced intestinal toxicity based on transcriptomic and metabolomic responses in human intestinal organoids. *Arch Toxicol* **95**, 2691–2718 (2021).
26. Rodrigues, D. *et al.* Unravelling Mechanisms of Doxorubicin-Induced Toxicity in 3D Human Intestinal Organoids. *Int J Mol Sci* **23**, (2022).
27. Powell, R. T. *et al.* deepOrganoid: A brightfield cell viability model for screening matrix-embedded organoids. *SLAS Discov* **27**, 175–184 (2022).
28. Bian, X. *et al.* OrgaNet: A Deep Learning Approach for Automated Evaluation of Organoids Viability in Drug Screening. *Lecture Notes in Computer Science (including subseries Lecture Notes in Artificial Intelligence and Lecture Notes in Bioinformatics)* **13064 LNBI**, 411–423 (2021).
29. Matthews, J. *et al.* OrganoID: a versatile deep learning platform for tracking and analysis of single-organoid dynamics. *bioRxiv* 2022.01.13.476248 (2022) doi:10.1101/2022.01.13.476248.
30. Wang, K. *et al.* Generative adversarial networks: Introduction and outlook. *IEEE/CAA Journal of Automatica Sinica* **4**, 588–598 (2017).

This work focuses on the development and validation of D-CryptO, a deep learning-based image analysis tool that can be used to analyze colon organoid structural maturity directly from brightfield images. D-CryptO can detect changes in organoid morphology over prolonged culture, during short-term perturbation, and following chemotherapeutic drug treatment.

L.A., J.X., A.S., A.C., J.G., S.R., N.A., H.M., B.Z*

D-CryptO: Deep learning-based analysis of colon organoid morphology from brightfield images

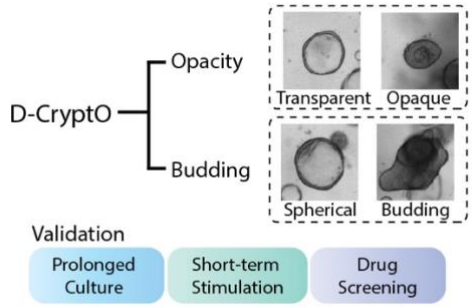

Supporting Information

D-CryptO: Deep learning-based analysis of colon organoid morphology from brightfield images

Lyan Abdul, Jocelyn Xu, Alexander Sotra, Abbas Chaudary, Jerry Gao, Shravanthi Rajasekar, Nicky Anvari, Hamidreza Mahyar, and Boyang Zhang[*]

Dose-dependent changes in organoid morphology

To further validate D-CryptO, we used it to assess the dose-dependent response of doxorubicin on opacity and budding following treatment at various concentrations. Doxorubicin is a chemotherapeutic that inhibits DNA and RNA synthesis and induces apoptosis.[30] We applied doxorubicin at concentrations of 50 µM, 5 µM, 0.5µM, 0.05 µM, and 0.005 µM **(Figure S1a)**. For opacity, the concentration at which 50% of organoids became opaque was 3.6 µM **(Figure S1b)**. For budding, the concentration at which 50% of the organoids still had budding structures was 39.8 µM **(Figure S1c)**. It is important to note that budding did not increase with higher dosages of doxorubicin. Instead, the percentage of non-viable organoids increased which was classified under the budding category. For diameter, the concentration at which 50% of the organoids had a reduction in diameter was 0.5 µM **(Figure S1d)**. Each parameter was impacted at different concentrations, indicating the importance of monitoring these features to assess drug toxicity.

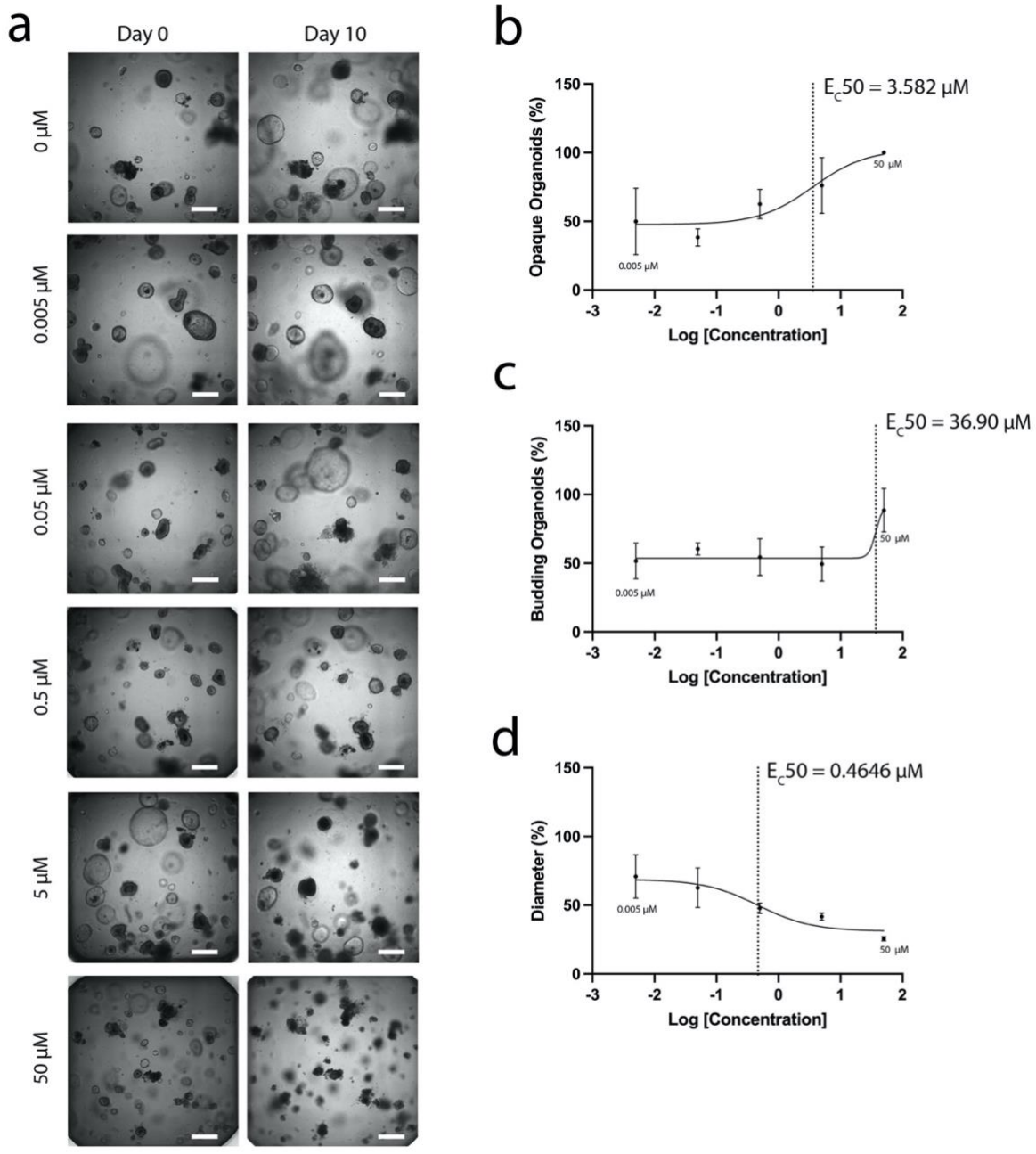

Supplementary Figure 1. Dose-dependent changes in organoid morphology. a, Brightfield images of organoids taken on Day 0 and Day 10 of drug treatment with doxorubicin at 5 different concentrations. Scale bar, 500 µm **b,** The percentage of opaque organoids following 10 days of treatment with increasing concentrations of doxorubicin. **c,** The percentage of budding organoids following 10 days of treatment with increasing concentrations of doxorubicin. **d,** The change in diameter following 10 days of treatment with increasing concentrations of doxorubicin.

Chapter 4: Conclusion

The work in the preceding chapters demonstrates the application of deep learning to analyze the morphology within three-dimensional tissue models. Specifically, the second chapter focuses on the detection and classification of morphologies within lung spheroids. When lung spheroids were cultured *in vitro*, they either self-assembled into polarized spheroids, with apical-basal polarity (referred to as "lumen") or into disorganized spheroids that did not exhibit polarity (referred to as "no lumen"). To apply deep learning to analyze the polarization of lung spheroids, a custom dataset containing examples of the two distinct spheroid structures was compiled and several pre-trained object detection models were trained on this dataset. The highest performing model was named Deep-LUMEN and was validated in two ways. First, we assessed how the extracellular matrix affects the ability of spheroids to assemble into polarized structures. The percentage of spheroids with polarized structures grown in Matrigel™ was significantly higher than those grown in different concentrations of fibrin. Second, we used Deep-LUMEN to study how the drug cyclosporin, which has previously been shown to induce cell toxicity, disrupts spheroid assembly. Even though spheroids were treated with a cyclosporin concentration that was sub-toxic, there was a significantly lower percentage of spheroids with lumens. Within these studies, three main conclusions were drawn. First, we showed that Deep-LUMEN can be used to accurately distinguish between the morphologies of interest. Second, we showed the importance of analyzing morphology. In both validation studies, although the spheroid structure was disrupted, the traditional parameters of diameter or the number of spheroids remained unaffected. Finally, we demonstrated that deep learning could facilitate the analysis of spheroid polarization.

Similarly, in the third chapter, deep learning was applied to analyze the complex morphology of another type of three-dimensional tissue model called an organoid. Colon organoids, which are derived from stem cells, can self-assemble into variable morphologies. Organoids differed in the extent of their budding and exhibited a range of opacities. The level of opacity and budding indicate the structural maturity of the organoid. To apply deep learning to assess organoid structural maturation, a dataset was created for the opacity feature (opaque or transparent organoids) and for the budding feature (spherical or budding organoids). Next, several pre-trained classification models were fit to the custom dataset and the model that performed with the greatest accuracy was called D-CryptO. D-CryptO was validated by analyzing colon organoid morphology over long-term culture. The analysis showed that there wasn't any significant variation in organoid morphology over time which can help improve the reproducibility of organoid studies. Additionally, D-CryptO could successfully capture changes in opacity and budding following short-term stimulation with forskolin. Furthermore, D-CryptO was validated by analyzing changes in morphology following treatment with chemotherapeutics to gain insights into the mechanisms of drug-induced toxicity. Overall, in this chapter, we demonstrated that deep learning could be applied to analyze more complex morphologies and we showed that we can apply our custom deep learning model in several cases.

Both chapters demonstrate that deep learning can be a valuable method to analyze three-dimensional tissue morphologies. This work is the first demonstration of analyzing the 3D structure using custom deep learning models. It can facilitate the analysis of other 3D tissue models so that greater insights into tissue physiology *in vivo* can be gained. In the work presented, both deep learning models and the custom datasets were made publicly available.

Some limitations of this method include the need for a large dataset which may not be possible for other types of tissue models. However, innovative techniques like data augmentation and the generation of new images with generative adversarial networks are also techniques that can be used to artificially increase the dataset.[30] Second, imaging artifacts like overlapping or blurry structures can reduce the accuracy of the models. Third, the work presented here did not use multiple instruments for imaging. Further studies should be done to assess the model accuracy across different instruments.

Future work could focus on adding a tracking feature to the deep learning models. Tracking can be used to monitor the assembly of 3D tissue models from a single cell to more complex morphologies. As a result, greater insights could be gained into the stages of morphological development and how external stimuli affect tissue assembly. Furthermore, these models could be packaged into interfaces that make them more accessible to individuals without programming experience. Nonetheless, the tools developed in this work permit tissue morphological analysis directly from images, in a non-destructive and high-throughput manner. They can be further developed to facilitate the structural analysis of other 3D tissues or be expanded for use in high-throughput drug screening pipelines.

List of References

1. Jensen, C. & Teng, Y. Is It Time to Start Transitioning From 2D to 3D Cell Culture? *Frontiers in Molecular Biosciences* **7**, 33 (2020).
2. Kola, I. & Landis, J. Can the pharmaceutical industry reduce attrition rates? *Nature Reviews Drug Discovery 2004 3:8* **3**, 711–716 (2004).
3. Torras, N., García-Díaz, M., Fernández-Majada, V. & Martínez, E. Mimicking epithelial tissues in three-dimensional cell culture models. *Frontiers in Bioengineering and Biotechnology* **6**, 197 (2018).
4. Ramaiahgari, S. C. *et al.* A 3D in vitro model of differentiated HepG2 cell spheroids with improved liver-like properties for repeated dose high-throughput toxicity studies. *Arch Toxicol* **88**, 1083–1095 (2014).
5. Mizuguchi, K. *et al.* Three-dimensional spheroid culture induces apical-basal polarity and the original characteristics of immortalized human renal proximal tubule epithelial cells. *Exp Cell Res* **404**, (2021).
6. Co, J. Y. *et al.* Controlling Epithelial Polarity: A Human Enteroid Model for Host-Pathogen Interactions. *Cell Reports* **26**, (2019).
7. Giles, R. H., Ajzenberg, H. & Jackson, P. K. 3D spheroid model of mIMCD3 cells for studying ciliopathies and renal epithelial disorders. *Nat Protoc* **9**, 2725–2731 (2014).
8. Kim, J., Koo, B. K. & Knoblich, J. A. Human organoids: model systems for human biology and medicine. *Nature Reviews Molecular Cell Biology 2020 21:10* **21**, 571–584 (2020).
9. Morizane, R. *et al.* Nephron organoids derived from human pluripotent stem cells model kidney development and injury. *Nat Biotechnol* **33**, 1193–1200 (2015).
10. Lancaster, M. A. *et al.* Cerebral organoids model human brain development and microcephaly. *Nature* **501**, 373–379 (2013).
11. Sato, T. *et al.* Long-term Expansion of Epithelial Organoids From Human Colon, Adenoma, Adenocarcinoma, and Barrett's Epithelium. *Gastroenterology* **141**, 1762–1772 (2011).
12. Sato, T. *et al.* Single Lgr5 stem cells build crypt-villus structures in vitro without a mesenchymal niche. *Nature 2009 459:7244* **459**, 262–265 (2009).
13. Shamir, L., Delaney, J. D., Orlov, N., Eckley, D. M. & Goldberg, I. G. Pattern Recognition Software and Techniques for Biological Image Analysis. *PLOS Computational Biology* **6**, e1000974 (2010).
14. Lecun, Y., Bengio, Y. & Hinton, G. Deep learning. *Nature 2015 521:7553* **521**, 436–444 (2015).
15. Kassis, T., Hernandez-Gordillo, V., Langer, R. & Griffith, L. G. OrgaQuant: Human Intestinal Organoid Localization and Quantification Using Deep Convolutional Neural Networks. *Scientific Reports 2019 9:1* **9**, 1–7 (2019).
16. Kegeles, E., Naumov, A., Karpulevich, E. A., Volchkov, P. & Baranov, P. Convolutional Neural Networks Can Predict Retinal Differentiation in Retinal Organoids. *Frontiers in Cellular Neuroscience* **14**, 171 (2020).
17. Lacalle, D. *et al.* SpheroidJ: An Open-Source Set of Tools for Spheroid Segmentation. *Comput Methods Programs Biomed* **200**, (2021).

18. Okuyama, H. *et al.* Dynamic Change of Polarity in Primary Cultured Spheroids of Human Colorectal Adenocarcinoma and Its Role in Metastasis. *The American Journal of Pathology* **186**, 899–911 (2016).
19. Vasquez, C. G., Vachharajani, V. T., Garzon-Coral, C. & Dunn, A. R. Physical basis for the determination of lumen shape in a simple epithelium. *Nat Commun* **12**, (2021).
20. Soetje, B., Fuellekrug, J., Haffner, D. & Ziegler, W. H. Application and Comparison of Supervised Learning Strategies to Classify Polarity of Epithelial Cell Spheroids in 3D Culture. *Frontiers in Genetics* **11**, 248 (2020).
21. Benning, L., Peintner, A., Finkenzeller, G. & Peintner, L. Automated spheroid generation, drug application and efficacy screening using a deep learning classification: a feasibility study. *Scientific Reports* **10**, 11071 (2020).
22. Abdul, L. *et al.* Deep-LUMEN assay – human lung epithelial spheroid classification from brightfield images using deep learning. *Lab on a Chip* **20**, 4623–4631 (2020).
23. Múnera, J. O. *et al.* Differentiation of Human Pluripotent Stem Cells into Colonic Organoids via Transient Activation of BMP Signaling. *Cell Stem Cell* **21**, 51-64.e6 (2017).
24. Crespo, M. *et al.* Colonic organoids derived from human induced pluripotent stem cells for modeling colorectal cancer and drug testing. *Nature Medicine 2017 23:7* **23**, 878–884 (2017).
25. Rodrigues, D. *et al.* New insights into the mechanisms underlying 5-fluorouracil-induced intestinal toxicity based on transcriptomic and metabolomic responses in human intestinal organoids. *Arch Toxicol* **95**, 2691–2718 (2021).
26. Rodrigues, D. *et al.* Unravelling Mechanisms of Doxorubicin-Induced Toxicity in 3D Human Intestinal Organoids. *Int J Mol Sci* **23**, (2022).
27. Powell, R. T. *et al.* deepOrganoid: A brightfield cell viability model for screening matrix-embedded organoids. *SLAS Discov* **27**, 175–184 (2022).
28. Bian, X. *et al.* OrgaNet: A Deep Learning Approach for Automated Evaluation of Organoids Viability in Drug Screening. *Lecture Notes in Computer Science (including subseries Lecture Notes in Artificial Intelligence and Lecture Notes in Bioinformatics)* **13064 LNBI**, 411–423 (2021).
29. Matthews, J. *et al.* OrganoID: a versatile deep learning platform for tracking and analysis of single-organoid dynamics. *bioRxiv* 2022.01.13.476248 (2022) doi:10.1101/2022.01.13.476248.
30. Wang, K. *et al.* Generative adversarial networks: Introduction and outlook. *IEEE/CAA Journal of Automatica Sinica* **4**, 588–598 (2017).